Fiorella Richard, P (Orcid ID: 0000-0002-0824-4777)
Poulsen Chris (Orcid ID: 0000-0001-5104-4271)

Seasonal Patterns of Water Cycling in a Deep, Continental Mountain Valley Inferred from Stable Water Vapor Isotopes

Richard P. Fiorella[1,2], Christopher J. Poulsen[1], Ashley M. Matheny[3,4]

1: Department of Earth and Environmental Sciences, University of Michigan, Ann Arbor, MI 48109

2: Department of Geology and Geophysics, University of Utah, Salt Lake City, UT 84112

3: Department of Civil, Environmental, and Geodetic Engineering, The Ohio State University, Columbus, OH

4: Department of Geological Sciences, University of Texas at Austin, Austin, TX

Corresponding author

Richard P Fiorella, rich.fiorella@utah.edu

Key Points

1) Stable water vapor isotopes respond to local and remote moisture sources in a continental setting and are best described by mixing models

2) Deuterium excess is a poor tracer of oceanic evaporation conditions in continental interiors as most vapor last evaporated over land

3) Local fluxes impact continental vapor d-excess all year, regional fluxes also impact winter d-excess when evapotranspiration is low

This is the author manuscript accepted for publication and has undergone full peer review but has not been through the copyediting, typesetting, pagination and proofreading process, which may lead to differences between this version and the Version of Record. Please cite this article as doi: 10.1029/2017JD028093

Corresponding author: Richard P Fiorella, rich.fiorella@utah.edu

Abstract

The origin of atmospheric moisture is difficult to determine from meteorological measurements alone. Stable water vapor isotopes can be used to trace the atmospheric history of water vapor, and therefore are a powerful tool for understanding water cycle processes across a range of spatial and temporal scales. We present sub-hourly measurements of summer and winter vapor isotope ratios from a deep mountain valley in northwestern Wyoming. Vapor isotopes are paired with local meteorological measurements, and relationships between local vapor isotopic compositions and large-scale air transport are explored using atmospheric back trajectories and a Lagrangian moisture source diagnostic. Isotopic compositions vary on diurnal to seasonal timescales, and to first order, track changes in local specific humidity. Local vapor isotopic composition varies with air transport pathway in both seasons, but cannot be uniquely mapped to a source region due to continental recycling of vapor. Diurnal variability in d-excess is substantial in summer, but not in winter. This seasonal contrast is likely driven by local surface and near-surface processes including evapotranspiration and boundary layer mixing, which partially overprint the source isotope ratios of the regional source during the summer and casts doubt on the use of d-excess over continental interiors as a tracer of evaporative conditions over the ocean. Continued monitoring of the isotopic composition of near-surface vapor in continental settings may help detect changes in regional moisture convergence and the local evapotranspiration flux, as well as assess meso-to-regional scale responses to hydrologic variability.

1 Introduction

Water exchange between continents and the atmosphere influences terrestrial climate and water resource availability (Seneviratne et al., 2010). Continental evapotranspiration (ET) amplifies terrestrial precipitation (van der Ent et al., 2010; Trenberth et al., 2006), and may moderate extreme event intensity (Diffenbaugh et al., 2015; J.-E. Lee et al., 2012; Seneviratne et al., 2014) and influence atmospheric circulation (Horton et al., 2015; Singh et al., 2016; Swann et al., 2012). These relationships are prone to change with Earth's hydrological cycle as it responds to atmospheric warming. In recent decades, ocean evaporation has increased (Yu & Weller, 2007), while continental pan evaporation has decreased (Liu et al., 2004; Roderick et al., 2007; Roderick & Farquhar, 2002) and vapor pressure deficit has increased (Ficklin & Novick, 2017; Novick et al., 2016). Measurements of continental humidity, however, provide little information on the processes that control the distribution of humidity or its variability. Therefore, observational tracers that can help distinguish between processes or sources are needed to diagnose the processes driving the variability and trend in these relationships.

Stable isotopes of hydrogen and oxygen have a long history as a water cycle process tracer (e.g., Bowen & Good, 2015; Gat, 1996). Phase changes unequally partition the heavy (e.g., $^{1}H_{2}{}^{18}O$, and $^{1}H^{2}HO$ or HDO) and light isotopologues (e.g., $^{1}H_{2}{}^{16}O$) of water, with the heavier isotopologues preferentially remaining in or entering the condensed phase (Gat, 1996). At equilibrium, this isotopic fractionation depends on temperature (Horita & Wesolowski, 1994; Majoube, 1971). Turbulent transport during evaporation can preclude isotopic equilibrium,

promoting an additional kinetic fractionation arising from the unequal diffusivities of water isotopologues (Cappa et al., 2003; Craig & Gordon, 1965; Luz et al., 2009; Merlivat & Jouzel, 1979) that most clearly appears in the deuterium excess parameter (d-excess, $d = \delta^2H - 8\delta^{18}O$) (Dansgaard, 1964).

For several decades, study of water isotopologues has focused on liquid and solid samples, as vapor isotopologue measurements were challenging (Ehhalt et al., 2005; Helliker et al., 2002; Rozanski & Sonntag, 1982; White & Gedzelman, 1984). The recent development of laser-based instruments capable of high-resolution (e.g., ~0.1-1 Hz) measurements of ambient water vapor isotope ratios, however, has opened the possibility of relatively facile, near-continuous monitoring of water vapor isotope ratios. Early applications of measurements of water vapor isotope ratios have included investigations of moisture source directions (Galewsky & Samuels-Crow, 2015; Steen-Larsen et al., 2015; Wei et al., 2016), upwind convective intensity (Brown et al., 2008; Samuels-Crow et al., 2014), passage of frontal systems (Aemisegger et al., 2015; X. Lee et al., 2006), cloud microphysical properties (Bailey et al., 2015; Galewsky et al., 2011), boundary layer entrainment and mixing with the free troposphere (Bailey et al., 2013; He & Smith, 1999; Lai & Ehleringer, 2010; Noone et al., 2013; Sodemann et al., 2017), ET (Aemisegger et al., 2014; Good et al., 2014; Welp et al., 2008), and dewfall or frost (Berkelhammer et al., 2013; Noone et al., 2013; Wen et al., 2012). These studies have established that water vapor isotope ratios are useful for understanding atmospheric moisture transport and land-atmosphere exchanges across a variety of time scales. and provide an

integrated picture of moisture transport from the ocean surface to continental interiors. The interpretation of water vapor isotope ratios at broad spatial and temporal scales, however, is complicated by the integrative nature of isotopic tracers, which may carry an array of signatures from upwind processes (e.g., Galewsky et al., 2016).

We pair measurements of the isotope ratios in near-surface water vapor in a deep, continental mountain valley in Northwestern Wyoming with local meteorological measurements and atmospheric back trajectories to help understand how these isotope ratio measurements vary with regional atmospheric circulation and local meteorology in the mountainous western US. We evaluate two hypotheses about the interpretation of water vapor isotopes in continental interiors. First, isotope ratios have canonically been interpreted to reflect, to first-order, a Rayleigh distillation process as vapor is lost from an air parcel (e.g., Rozanski et al., 1993). Several water vapor isotope studies, however, have identified atmospheric mixing better describes variability in atmospheric water vapor isotope ratios. We also find that mixing of vapor sources is a dominant atmospheric process for both seasons. Second, d-excess values have traditionally been considered to reflect evaporative conditions over the ocean (e.g., Benetti et al., 2014; Craig & Gordon, 1965; Pfahl & Wernli, 2008; Uemura et al., 2008), and to be quasi-conserved during subsequent Rayleigh condensation over continents (e.g., Gat, 1996). This assumption has been challenged by observations of distinct diurnal and synoptic variations in continental vapor d-excess that cannot be explained by variability in oceanic conditions and instead likely reflect contributions from ET (e.g., Aemisegger et al., 2014; Lai & Ehleringer, 2010; Simonin et al.,

2014; Welp et al., 2012). Likewise, we find a strong diurnal d-excess cycle during the summer, but little diurnal variability during the winter, suggesting that the ET flux exerts a strong control on isotope ratios in low-level water vapor. Using a Lagrangian moisture tracer, we find that most of the moisture arriving to the field site last evaporated over land, indicating that any isotopic signal imparted from ocean evaporation has likely been overprinted by continental ET. We suggest that d-excess instead reflects the parcel-integrated conditions of last evaporation, and its variability provides information on the relative importance of oceanic and continental moisture inputs in continental settings.

2 Methods

2.1 Site Description

The Camp Davis Rocky Mountain field station (CDFS, Fig. 1, 43.283°N, 110.659°W) occupies 48.6 ha in a NW-SE trending mountain valley in Wyoming and is located at 1860 m ASL. The valley is 10 km long and 2 km wide at its widest point, bisected by the Hoback River, and bordered by the Bridger-Teton National Forest. Elevations of the surrounding ridges range between 2100-3000+ m. Long-term climatological records are not available at the CDFS, but mean annual temperature and mean annual precipitation at the nearby NOAA climate stations in Bondurant, WY (1992 m elevation, 20 km ESE) and Jackson, WY (1892.8 m elevation, 25 km NNW) are 1.5°C and 4.1°C, and 480 mm and 430 mm, respectively (NCDC 1981-2010 climate normals). Winter precipitation is typically associated with extratropical cyclones and northwesterly vapor transport, while summer precipitation is often convective and fed by

moisture transport from the west and the southwest (Despain, 1987). Nocturnal valley inversions, which commonly occur in deep valleys in the Rocky Mountains (Whiteman, 1982; Whiteman et al., 2004), occur throughout the year. Thermal inversions can persist for several days during the winter (e.g., Whiteman et al., 1999).

2.2 Meteorological measurements

Meteorological data were collected at a 10-m tower. Measurements included 2- and 10-m temperature and relative humidity (RH) (CS500, Campbell Scientific/Vaisala), 10-m wind speed and direction (05103, R.M. Young), barometric pressure (CS100, Campbell Scientific/Setra), downwelling shortwave radiation (LI200S, LI-COR Biosciences), and precipitation amount (TE525WS, Texas Electronics). Sensor data were recorded every minute by a Campbell Scientific data logger (CR10X) and averaged or summed to 15-minute intervals.

2.3 Vapor isotope measurements

We deployed a Picarro L2120-i cavity ring-down spectrometer (CRDS) at the CDFS for one winter and two summer periods: 12 June-2 September, 2012 (DOY 165-247); 12 January-2 February, 2013 (DOY 13-35); and 30 June-15 July, 2014 (DOY 181-197). The CRDS measured ambient water vapor $\delta^{18}O$ (‰), $\delta^{2}H$ (‰), and specific humidity (q, ppm) at ~1 Hz from a sampling height ~3 m above the ground. The location of the CRDS analyzer changed throughout the campaigns due to logistical constraints but was always located within non-forested clearings.

During summer 2012, the analyzer was initially deployed in a cabin ~150 m south of the CDFS meteorological tower, and then moved into a small temperature-controlled shed constructed 15 m away from the tower. All subsequent summer isotope measurements were collected in the temperature-controlled shed next to the tower. Winter measurements were made in a building closer to the wall of the valley, ~200 m southwest of the meteorological tower. The Hoback River was always more than 200 m away.

Vapor was introduced to the CRDS through 1/8" stainless steel tubing (prior to construction of the temperature-controlled shed in summer 2012), or through Bev-A-Line IV plastic tubing. Prior studies have indicated that memory effects caused by adsorption of water vapor to tubing walls of these materials is minimal (Simonin et al., 2013; Tremoy et al., 2011). A partial vacuum was maintained in the sampling lines to ensure vapor in the sampling line represented current conditions and reduce the likelihood of water condensation in the tubing. Sampling lines were not heated, and we observed no evidence of condensation within the sampling lines. Vapor isotope data presented here are 15-minute averages. Isotope ratios are reported in delta notation as permil deviations from the VSMOW international standard (e.g., Coplen, 1996). Deuterium excess (d-excess) is calculated after Dansgaard (1964) ($d = \delta^2H - 8\delta^{18}O$).

Raw instrument isotope values were calibrated in two steps. First, analyzer measurements were corrected for an apparent isotope ratio bias that varies with cavity humidity (e.g., Aemisegger et al., 2012; Schmidt et al., 2010; Sturm & Knohl, 2009). Two water standards were

measured across cavity humidities ranging from 2,000 to 30,000 ppmv, we then fit a hyperbola to determine isotopic correction as a function of cavity humidity (Text S1, Fig. S1). Ambient humidity during the winter period often fell below 2,000 ppmv, which imparts an uncharacterized uncertainty to these measurements since they fall outside the bounds of our humidity calibration. We assume that as the magnitude of the isotopic corrections is large at low humidity values (Fig. S1), extrapolating this humidity calibration is preferable to omitting this correction at low humidity values. Excluding periods where analyzer humidity fell below 2,000 ppm does not alter the conclusions presented here, and removing these periods risks filtering observations corresponding to real environmental conditions. A sensitivity analysis is provided in the Supporting Information (Text S2). Second, the humidity-corrected isotope measurements were standardized to the VSMOW-VSLAP using two lab standards with known isotope ratios. We measured two liquid water standards every 12 hours to monitor for instrumental drift and calibrate measurements to the VSMOW/VSLAP scale (Coplen, 1996). For the 2012 and 2013 campaigns, standards were introduced using an autosampler, while the Picarro Standard Delivery Module was used for the 2014 campaign. Typical analytical precision is 0.1‰ for $\delta^{18}O$ and 0.4‰ for $\delta^{2}H$. Apparent instrumental drift was similar to the analytical precision; therefore, no drift corrections were applied.

2.4 Process-based isotope modeling

Evaporation, condensation, and air-mass mixing promote characteristic patterns of isotopic change with respect to changes in humidity (e.g., Dessler & Sherwood, 2003; Galewsky & Hurley, 2010; Gat, 1996; Noone, 2012). The canonical Rayleigh distillation equation describes an open condensation process, where all of the condensed liquid is immediately removed from the air parcel (Gat, 1996). The isotopic composition of water vapor in a condensing air mass undergoing Rayleigh distillation will be proportional to the natural logarithm of specific humidity (Dansgaard, 1964; Gat, 1996):

$$(\alpha - 1)\ln\left(\frac{q}{q_0}\right) = \ln\left(\frac{R}{R_0}\right) \approx (\delta - \delta_0) \#(1)$$

where q is the specific humidity, R is the heavy-to-light isotope ratio, δ is the isotopic composition expressed as a permil deviation from a standard R (VSMOW for water, Coplen, 1996), and α the effective isotope fractionation factor. A subscript *0* refers to the initial properties of the parcel. The effective isotope fractionation factor may be altered by temperature-dependent changes in the equilibrium fractionation factor (Horita & Wesolowski, 1994; Majoube, 1971), or by variability in the kinetic fractionation factor with RH, temperature, and wind speed (Merlivat & Jouzel, 1979; Pfahl & Sodemann, 2014). Equation 1 assumes constant α throughout condensation; this assumption may be relaxed when solved numerically with variable α for small changes in q/q_0 (e.g., Noone, 2012).

For a closed condensation process, all of the condensate remains within the air parcel, and the total water content of the air parcel remains unchanged. In this case, isotopic

composition of water vapor in an air parcel is linearly proportional to the specific humidity (Jouzel, 1986; Noone, 2012):

$$\left(\frac{q}{q_0} - 1\right)(\alpha - 1) \approx \delta - \delta_0 \#(2)$$

Condensation processes with a partial loss of condensate will result in isotope ratios intermediate to these two end-member models. In contrast, local or upwind partial evaporation of falling raindrops and ET can preferentially return light water isotopologues to the atmosphere, causing vapor to be more depleted in heavy isotopologues than predicted from condensation processes (J.-E. Lee & Fung, 2008; Risi et al., 2008; Stewart, 1975). These processes can be modeled by inflating the fractionation factor used in equation 1 to account for the return of lighter isotopologues during evaporation ("super-Rayleigh" condensation, Noone, 2012):

$$[(1 + \phi)\alpha - 1]\ln\left(\frac{q}{q_0}\right) = \ln\left(\frac{R}{R_0}\right) \#(3)$$

Finally, the mixing of two or more air masses can be modeled from mass balance. Using separate mass balance equations for the light and heavy isotopes, the observed specific humidity can be expressed as the sum of contributions of moist and dry air masses with distinct isotope ratios:

$$(1 - R_{obs})q_{obs} = (1 - R_{moist})q_{moist} + (1 - R_{dry})q_{dry} \ \text{(light isotope mass balance)} \#(4)$$

$$R_{obs}q_{obs} = R_{moist}q_{moist} + R_{dry}q_{dry} \ \ \text{(heavy isotope mass balance)} \#(5)$$

where subscripts *obs*, *moist*, and *dry* refer to the observed, moist, and dry components respectively. These equations can be simplified by noting that $R << 1$ for all three components,

and that the heavy isotope mass balance equation can be written in delta notation equivalently within 0.01‰ (Hayes, 1982):

$$q_{obs} = q_{moist} + q_{dry} \#(6)$$

$$\delta_{obs} q_{obs} = \delta_{moist} q_{moist} + \delta_{dry} q_{dry} \#(7)$$

Combining these mass balance equations into one equation for the observed water vapor isotope ratios yields:

$$\delta_{obs} q_{obs} = \delta_{moist} q_{obs} + \left(\delta_{dry} - \delta_{moist}\right) q_{dry} \#(8)$$

This model is analogous to the Keeling plots used to discriminate sources and sinks of CO_2 to the atmosphere (Keeling, 1958, 1961; Miller & Tans, 2003; Pataki et al., 2003), and has been previously extended to atmospheric water vapor to investigate mixing of atmospheric air masses (Dessler & Sherwood, 2003; Galewsky & Hurley, 2010; Gedzelman, 1988; Noone et al., 2011), and to constrain surface fluxes from natural ecosystems (He & Smith, 1999; Noone et al., 2013), agricultural fields (Brunel et al., 1992; Welp et al., 2008), and estimate urban combustion vapor emissions (Fiorella et al., 2018).

We applied each of these isotope models to the CDFS isotopic and meteorological time series by calculating moving correlations between: (a) q and $q\delta$ (air-mass mixing), (b) ln(q) and δ (Rayleigh condensation), and (c) q and δ (closed condensation).

Each correlation was calculated over a 96-point moving window, corresponding to 24 hours of data. We divided the data into three classes where the dominant process observed at the CDFS was: (1) air-mass mixing, (2) condensation (Rayleigh or closed), and (3) neither. A process was

considered "dominant" when the coefficient of determination (e.g., r^2) was greater than 0.8 and greater than the r^2 for alternate process models (after Noone et al., 2011). Correlation differences between Rayleigh and closed system condensation were small (Fig. S2); therefore, condensation was considered dominant if either the Rayleigh or closed models met these requirements. We assumed no process was dominant when the r^2 was less than 0.8 for all process models.

We constructed idealized models for condensation or air-mass mixing between moist oceanic and dry continental end-members (after Noone, 2012). Ocean temperatures of 25°C or 10°C were used to estimate the saturation specific humidity and isotopic composition of vapor in equilibrium with sea water ($\delta^{18}O_{seawater} \equiv \delta^{2}H_{seawater} \equiv 0‰$) for the moist end member. These moisture conditions were chosen to simulate conditions typical of the northern (10°C source) and subtropical Pacific Ocean (25°C) and are provided primarily for orientation. For the air-mass mixing model, the oceanic end member is mixed with a dry continental end member with q = ~0.1 mmol mol^{-1} and $\delta^{18}O$ = -95‰; dry end-member compositions were estimated by assuming the dry air mass had nearly all of its moisture removed through Rayleigh distillation. Following this mixing line, we simulate condensation under open/Rayleigh and closed system conditions starting from 90% RH at the initial parcel temperature (25°C or 10°C).

2.5 Atmospheric back trajectory analysis

We calculated atmospheric back trajectories to investigate large-scale patterns in moisture advection to northwestern Wyoming using the HYbrid coordinate Single Parcel Lagrangian Integrated Trajectory model (HYSPLIT, Draxler & Hess, 1998). HYSPLIT trajectories were

calculated using three meteorological data sources: (1) the North American Regional Reanalysis North American Regional Reanalysis (NARR, Mesinger et al., 2006), (2) the Global Data Assimilation System (GDAS), and (3) the NCEP/NCAR reanalysis (Kalnay et al., 1996). Trajectories were initiated from five locations (CDFS and points displaced 0.25° in each cardinal direction) at 250, 500, 1000, 1500, and 2000 m above the ground surface, resulting in sets of 25 trajectories calculated for each time slice. Sets of 10-day back trajectories were initiated every six hours during the measurement periods, with hourly estimates of the parcel position, its specific humidity, and PBL height at location and time. Vertical velocities were derived from wind-source inputs. Back trajectories were assigned to one of five regions: (1) the Snake-Columbia plain and the northern Pacific (north Pacific), (2) trajectories crossing the Sierra Nevada before arriving at the CDFS (High Sierra), (3) the southwestern US and the subtropical Pacific (subtropical Pacific), (4) predominantly continental south of the CDFS, including the Gulf of Mexico (southern continental), and (5) predominantly continental north of the CDFS, including the Canadian Arctic (northern continental) (Fig. 1). These source regions are similar precipitation source regions identified for the adjacent Great Basin (Friedman et al., 2002; Houghton, 1969). Trajectories were assigned to the region the parcel occupied for the longest period of time. Mean cluster q, $\delta^{18}O$, and d-excess values were determined for each cluster to assess if local isotope observations at the CDFS from these five regions were distinct.

Within each of these source regions, remote moisture contributions to the CDFS were identified using the Lagrangian tracer of Sodemann et al. (2008). Briefly, this tracer identifies

moisture sources to an air parcel by tracking the parcel specific humidity change throughout the back trajectory, and apportions moisture additions along the trajectory into increases occurring within the PBL (*f*) or above the PBL (*e*). Hourly changes in humidity are calculated from the HYSPLIT extracted specific humidity values. Starting from the beginning of each back trajectory and iterating forward in time, the fractional contributions *f* and *e* to a moisture addition event *n* are calculated as:

$$f_n = \frac{\Delta q_n}{q_n}, e_n = 0 \ (if \ n \ in \ PBL) \#(9)$$

$$e_n = \frac{\Delta q_n}{q_n}, f_n = 0 \ (if \ n \ above \ PBL) \#(10)$$

The parameters f_n and e_n are calculated for each moisture addition event *n* with $\Delta q \geq 0.1$ g/kg. If more than one moisture addition occurs along a trajectory, prior additions are recalculated to reflect their reduced contribution to the air parcel:

$$f_m = \frac{\Delta q_m}{q_n}, e_m = \frac{\Delta q_m}{q_n}, \text{for } t(m) < t(n) \#(11)$$

where *t* is time, *n* refers to the current event, and *m* refers to all moisture addition events in the trajectory prior to the time of event *n*. Conversely, if the parcel humidity decreases along the trajectory (e.g., $\Delta q < 0$ g/kg), it is assumed to be precipitation, and all prior moisture addition masses must be reduced by a proportional amount:

$$\Delta q'_m = \Delta q_m + \Delta q_n f_m, \text{for } t(m) < t(n) \#(12)$$

where $\Delta q'_m$ refers to the updated moisture addition amounts for all prior times. The remaining fractional contribution that cannot be assigned to moisture additions within (*f*) or above (e*)* the

PBL is denoted *d*. Integration through time yields a total contribution from PBL sources (f_{tot}), sources above the PBL (e_{tot}), and unattributable sources (d_{tot}); these three parameters sum to one by definition. HYSPLIT-extracted PBL heights were scaled by a factor of 1.5, following Sodemann et al. (2008), though in contrast to its original formulation, we applied this algorithm hourly instead of in 6-hour intervals since HYSPLIT provides hourly position and meteorology estimates. A shorter time step and a PBL scaling of 1.5 generally decrease the unattributed and above-PBL fractions (*d* and *e*), and increase the within-PBL attributed fraction *f* (Fig. S3). We assumed the minimum PBL height to be 500 m AGL, to reduce the spread between inferred moisture sources across the GDAS, NCEP, and NARR datasets arising solely from differences in the PBL parameterizations. NCEP and GDAS PBL heights along the trajectory often approached zero, while PBL heights derived from the NARR dataset were on average ~500 m higher than NCEP or GDAS PBL heights (Fig. S4). Again, increasing minimum PBL height tended to increase the proportion of moisture additions attributed within the PBL at the expense of above-PBL additions (Fig. S5). The mean parcel position between time t and t-1 was assumed to be the location of moisture addition for within PBL additions, and these amounts were aggregated to a 1.0° grid and weighted by their contribution to the parcel humidity at CDFS (e.g., $f*q_{CDFS}$). Moisture addition locations cannot be determined for the above-PBL and attributable fractions. Remotely-diagnosed moisture sources are used to estimate a mass-weighted RH at the evaporative source, which we compare to the CDFS vapor d-excess value. D-excess is highly sensitive to the RH at the evaporative source (Craig & Gordon, 1965; Jouzel et al., 1982;

Merlivat & Jouzel, 1979; Pfahl & Sodemann, 2014), and we use relationships between remote and local RH with CDFS d-excess to infer the relative importance of local and remote fluxes in driving water vapor isotope ratio variability at the CDFS.

3 Results

3.1 Seasonal and interannual variability

Summer vapor was less depleted in heavy isotopologues than winter vapor (Fig. 2-4). Mean vapor $\delta^{18}O$ ($\delta^{2}H$) isotope ratios for summer 2012, winter 2013, and summer 2014 were -19.8‰ (-155.4‰), -33.5‰ (-251.5‰), and -20.5‰ (-164.2‰) respectively (Table 1). Mean vapor d-excess was lower in summer (3.3 and 0.0‰ for 2012 and 2014) than winter (16.8‰). Isotope ratios ranged from -29.3‰ (-224.2‰) to -9.6‰ (-82.1‰) for $\delta^{18}O$ ($\delta^{2}H$) in summer 2012, -24.6‰ (-195.4‰) to -14.9‰ (-129.5‰) in summer 2014, and -38.6‰ (-289.4‰) to -25.1‰ (-188.3‰) in winter 2013. Winter conditions were drier and averaged ~25°C colder than summer conditions (Table 1). Summer 2-m air temperatures ranged from -2.6°C to 33.6°C in 2012 (Fig. 2d) and 0.0°C to 30.9°C in 2014 (Fig. 4d), while winter 2013 temperatures ranged from -30.5°C to 5.5°C (Fig. 3d). Summer 2-m specific humidity varied more than winter specific humidity. Specific humidity varied between 1.4 and 14.6 g/kg during summer 2012 (Fig. 2e) and between 2.4 and 16.6 g/kg during summer 2014 (Fig. 4e); in contrast, the specific humidity varied between 0.3 and 4.6 g/kg during winter 2013 (Fig. 3e).

The relationship between $\delta^{18}O$ and $\delta^{2}H$, which covary strongly in meteoric waters globally along the global meteoric water line (GMWL) (Craig, 1961), also varied seasonally and interannually (Fig. 5). The vapor local meteoric water line (LMWL) for summer 2012 was $\delta^{2}H = (7.53\pm0.05)\delta^{18}O - (5.97\pm0.95)$ ($r^2 = 0.812$) and for summer 2014 was $\delta^{2}H = (4.93\pm0.18)\delta^{18}O - (63.06\pm3.78)$ ($r^2 = 0.360$). Summer vapor isotope ratios showed wide variability in $\delta^{18}O$-$\delta^{2}H$ space, with the majority of the data points plotting below the GMWL. In contrast, the winter data occupy a narrow band close to and mostly above the GMWL. The vapor LMWL during the winter 2013 observation period was $\delta^{2}H = (7.21\pm0.02)\delta^{18}O - (9.34\pm0.71)$ ($r^2 = 0.983$). The weaker correlation between $\delta^{18}O$ and $\delta^{2}H$ during summer compared to winter hints at greater complexity in the summer water cycle, and seasonally distinct relationships between isotopic compositions, local meteorological conditions, and large-scale moisture transport.

3.2 Relationships between isotopic composition, specific humidity, and condensation and mixing

Clear seasonal contrasts emerged in the relationship between q and $\delta^{18}O$ or $\delta^{2}H$ (Fig. 6). For both seasons, there was substantial variability in δ for a given q (Fig. 6). Comparing the $q\delta^{18}O$ distributions to their model-predicted values assuming a warm ocean source (25°C), the majority of data fell between Rayleigh and closed-system condensation pathways for summer 2012 (62.1%) and winter 2013 (52.2%), though only 16.3% of data points fell within these models for summer 2014 (Fig. 6a, Table 2). Instead, most summer 2014 data points were too depleted in

heavy isotopes to be consistent with Rayleigh condensation (83.5%), which was the second most common outcome for summer 2012 (33.7%) and winter 2013 (30.9%) (Table 2). The remaining observations for all three seasons fell between the closed condensation and mixing models (Fig. 6). If a cold ocean source was assumed (10°C), most CDFS observations were too moist or too depleted in heavy isotopes to be adequately explained by these models (Table 2).

Correlation analysis on daily timescales identified air-mass mixing as the dominant process influencing near-surface water vapor isotope ratios (>75% for summer, >95% for winter, Table 3, Fig. S2). Air-mass mixing remained the dominant process at the CDFS regardless of the size of the correlation window (Table S2). The importance of mixing was also apparent in the linear relationships observed in a q vs $q\delta^{18}O$ or $q\delta^{2}H$ plot (Fig. 6c,d), which clearly deviate from non-linear trends that would be expected for the condensation models. This pattern highlights that though continental isotope ratios generally follow a relationship similar to Rayleigh distillation, our high-frequency measurements more likely reflect the mixture of two or more partially condensed air masses. Variations in the slope of this relationship across timescales of days to weeks likely represent changes in the isotope ratios of vapor mixing into the near-surface atmosphere at the CDFS through changes in advected vapor and/or local ET isotope ratios. Likewise, values located between two different condensation lines may result from upwind mixing of two distinct air-masses, or from condensation processes where only a fraction of condensate leaves the parcel as precipitation (e.g., Bailey et al., 2015).

A seasonal estimate of the mean parcel characteristics undergoing mixing can be estimated from the relationships between $q\delta$ and q (Fig. 6c,d). The most parsimonious model across both winter and summer suggests mixing between a moist end-member, with characteristics consistent with a "super-Rayleigh" (Equation 3, $\phi[\delta^{18}O] = 0.01$, $\phi[\delta^{2}H] = 0.08$) condensation process, and a dry end-member that has nearly lost all of its water vapor through condensation. Summer 2012 data suggest a moist end-member with an isotopic composition of ~ -15‰ for $\delta^{18}O$ (Fig. 6c) and ~ -115‰ for $\delta^{2}H$ (Fig. 6d, Eq. 8). Summer 2014 and winter 2013 data both suggest greater upwind condensation, with ~40% and ~70% of the initial oceanic parcel moisture content having condensed out prior to mixing respectively, suggesting end-member isotopic compositions of ~ -19‰ $\delta^{18}O$ (Fig. 6c) and ~ -153 ‰ $\delta^{2}H$ (Fig. 6d) for summer 2014 and ~ -30‰ $\delta^{18}O$ (Fig. 6c) and ~ -255‰ $\delta^{2}H$ (Fig. 6d) for winter 2013. This is the simplest depiction of the atmospheric processes determining the end-member characteristics; in reality, a variety of condensation or mixing processes may produce these end members.

3.3 Relationships between air source pathways and CDFS vapor isotope ratios

Large, low-frequency (e.g., period of days) variability in specific humidity and isotopic composition occur in both the summer and the winter. We analyzed 10-day atmospheric back trajectories to determine if these low-frequency variations relate to air source pathway (Fig. 1). For all three seasons, advection was most commonly from the northern Pacific region, followed by advection from the northern continental and subtropical Pacific regions (Table 4). Advection

from the north Pacific comprised 48-60% of the summer 2012 record and 70-81% of the winter 2013 and summer 2014 records. During summer, back trajectories derived from NCEP indicated more frequent air advection from the northern Pacific and less from the southern Pacific than back trajectories derived from GDAS or NARR, which may be related to the coarser resolution of the NCEP product and greater truncation of the Cascade mountains. Advection from the subtropical Pacific region comprised 31-42% of the summer 2012 record, but only 9-17% of the winter 2013 and summer 2014 records. Advection from the northern continental region comprised <10% of the back trajectories during summer 2012 and winter 2013 periods but was 13-19% of the summer 2014 record. Advection over the High Sierra or from the southern continental region was infrequent (< 5% for all seasons) (Table 4). Precipitation was associated with the moister air source pathways. In summer 2012, ~42% of the seasonal precipitation occurred when air was sourced from the south, despite advection from the south occurring only 9-33% of the time (Table 4). Likewise, in summer 2014, ~70% of precipitation was associated with advection from the northern continental region, despite advection occurring from this region only 13-19% of the period of record. Yet despite these clear tendencies driven by air source region, the humidity and isotope ratio distributions overlap substantially across all seasons (Fig. 7a-c). Therefore, vapor measurements at the CDFS cannot confidently be attributed uniquely to one of the five source regions defined above following Friedman (2002) and Houghton (1969).

Additionally, d-excess distributions suggest a substantial seasonal difference in the vapor sources to the CDFS. (Fig. 7d-f). Summer d-excess distributions from the major air source

regions are broad, bimodal, and overlapping (Fig. 7d-e). For each of these distributions, one of the modes occurs at a positive d-excess value, while the other mode occurs at a negative d-excess value. The positive mode occurs during the day, while the negative mode reflects nighttime conditions (Fig. 7d-e), suggesting that diurnal processes and vapor sources at the CDFS may contribute strongly our isotopic observations during summer. Two air source regions, High Sierra and southern continental, do not fit this pattern in summer 2012. As these are minor contributors to advection to the CDFS, this deviation likely reflects a bias introduced by the limited sampling period in terms of length of record and time of day. In contrast, winter d-excess distributions are narrow and unimodal, but are not distinct (Fig. 7f). The narrower distribution d-excess in the winter suggests that the local diurnal cycle at CDFS has little impact on winter vapor isotope ratios.

3.4 Sources of vapor to the CDFS and their impact on d-excess

The vapor d-excess record at CDFS and its variability suggest a seasonal change in the roles that advected water vapor and local ET have in influencing surface vapor isotope ratios. We examine this pattern in this section by: 1) mapping remote moisture sources to the CDFS using the Lagrangian moisture tracer of Sodemann et al. (2008), 2) extracting a mass-weighted mean RH from remote sources, and 3) comparing the relationships between CDFS d-excess and local and remote RH. Two important features are apparent from the moisture uptake footprints generated from this tracer (Fig. 8). First, moisture uptake locations over the ocean are similar

across air source regions with trajectories reaching the ocean. This trend likely indicates that differences between these parcels when they reach the CDFS reflects differences in conditions over the land surface, and whether they are forced over high topographic barriers. Parcels are forced over the Sierra Nevada when wind speeds are strong enough to overcome atmospheric stratification (Galewsky, 2009; Lechler & Galewsky, 2013). Similar trends are found for trajectories using all three data sources (Fig. S6-7). Together, these observations suggest that isotopic variability imparted through differences in oceanic source may be more muted than anticipated.

Second, remotely-diagnosed contributions to CDFS humidity are higher over land than over the ocean, by up to three orders of magnitude (Fig. 8). During northerly or westerly advection, maximum contributions are focused along the Snake River Plain, while maximum contributions concentrate along the western edge of the Wasatch Plateau if advection is from the south. Continental moisture recycling may substantially reduce the ocean-derived fraction of vapor arriving at the CDFS, further weakening ties between oceanic evaporation conditions and CDFS isotope ratios. If the PBL-derived fraction of moisture (f_{tot}) is subset into land and ocean components, the land contribution usually dominates (Fig. 9). PBL-diagnosed oceanic moisture rarely exceeds a 25% contribution, while moisture from land PBL sources often comprises 40-90% of the attributed humidity (Fig. 9).

High contributions of land-derived moisture to CDFS humidity are present across all three back trajectory data sources, though there are distinct differences across these data sources.

Oceanic contributions to CDFS humidity are smallest in the NARR and GDAS back trajectories (Fig. 9a-f) but are larger in the NCEP back trajectories (Fig. 9g-i). Likewise, the fraction of vapor that cannot be attributed along the back trajectory is generally negligible in the NARR and GDAS back trajectories (< 5%, Fig. 9a-f), but often exceeds 25% in the NCEP back trajectories. These patterns indicate a clear difference in moisture transport simulated by NCEP compared to GDAS or NARR. PBL moisture from land ET remain a greater fraction of CDFS humidity than ocean evaporation for all three back trajectory data sources if no minimum PBL height is specified (Fig. S8), or if above-PBL uptakes are assumed to result from local shallow convection (forcing e=0, and attributing all Δq into f, cf., Aemisegger et al., 2014) (Fig. S9). As a result, a strong relationship would be expected between CDFS d-excess and the RH of remotely-diagnosed moisture for land evaporative sources, but perhaps not for ocean evaporative sources.

Correlations of CDFS d-excess with remote-diagnosed RH at the evaporative site generally match these expectations (Fig. 10). Few significant relationships between oceanic RH and 24-hour running average CDFS d-excess are found (Fig. 10a-c). We find significant relationships between remote land RH and d-excess for evaporation for all three back trajectory data sources in summer 2012 and winter 2013 (Fig. 10d-e), though no significant relationships are observed during summer 2014 (Fig. 10f), perhaps due to the shorter duration of the record. Interestingly, the slope of the relationship between land-diagnosed RH and CDFS humidity during summer 2012 is positive, suggesting greater kinetic fractionation when humidity is high. We suggest that this may result from a weak moisture advection to the CDFS, assuming some

spatial correlation in humidity between CDFS and the surrounding region, which could promote a larger cycle in d-excess and RH at CDFS, and produce a lower 24-hour mean d-excess value.

We observe a significant relationship between CDFS d-excess and local RH during all three seasons (Fig. 10j-l). This local relationship is substantially stronger during the summer, and possesses a higher magnitude slope (~ -0.4‰ /%RH for summer, -0.10‰ / %RH for winter, Fig. 10j-l). These relationships suggest that local vapor fluxes are significant contributors to CDFS humidity and vapor isotope ratios, but that the impact of local vapor fluxes is greater in summer than winter.

4 Discussion

To first order, seasonal contrasts in water vapor isotope ratios follow changes in specific humidity (Fig. 2-6). Variability in isotope ratios at the CDFS is usually best described by models of air-mass mixing rather than condensation models (Fig. 6, Table 3), though the isotope ratios of mixing end-members may be set by condensation or evaporation locally or along the parcel trajectory to the CDFS. For example, observations generally suggest a moist end-member with isotopic compositions set via a “super-Rayleigh” process, though the precise nature of the processes giving rise to observed CDFS vapor isotope ratios cannot be determined by point measurements due to the integrative nature of water vapor isotope ratios. Mean seasonal properties of the moist end-member vary from summer to winter, and likely reflect changes in both the intensity of the local ET flux, but also regional-scale changes in evaporation and condensation. Advection from different air source regions may nudge the distributions of

humidity and its isotopic composition at the CDFS, but the CDFS observations cannot be uniquely inverted to their dominant source region. The strong seasonal contrast in the distributions and diurnal cycles of vapor d-excess, however, may be more useful for assessing whether local fluxes or regional advection have a stronger influence on near-surface vapor isotope ratios at the CDFS.

Imprints of both local meterological and regional advective processes are observed in vapor isotope ratios at the CDFS. On daily to weekly timescales, individual weather systems can have a dramatic impact on the isotope ratios of near-surface vapor (e.g., Aemisegger et al., 2015; X. Lee et al., 2006; White & Gedzelman, 1984). For example, the first eleven days of our winter measurements were dominated by dry, clear, and cold conditions (Fig. 3). During this period, vapor was most depleted in heavy isotopologues during the study due to air advection from the dry, cold north (Fig. 8) combined with local conditions that were very cold (Fig. 3). Abrupt changes in summer vapor isotope ratios are also observed, such as with precipitation events (e.g., Fig. 2,4). Rapid increases in humidity and vapor isotope ratios during precipitation events are expected due to strong moisture convergence and subcloud evaporation of precipitation formed from moist, less isotopically-depleted air masses (J.-E. Lee & Fung, 2008; Risi et al., 2008). Yet, despite clear fingerprints of regional-scale processes in our isotope ratio measurements, isotope measurements at the CDFS cannot be uniquely inverted to moisture source regions, perhaps due to variability in remote source region conditions or in the impact of local ET fluxes and the integrative nature of water isotope tracers.

However, a dramatic difference in d-excess trends are observed for summer compared to winter, which indicates that d-excess may be a more sensitive recorder of terrestrial hydrologic processes. Correlations between CDFS and local or remotely-diagnosed moisture source region RH indicate that local RH always influences vapor d-excess (Fig. 10g-i). The magnitude of change and strength of correlation between d-excess and local RH is greater in the summer, which may reflect a stronger role for local fluxes of water vapor, such as local ET, during the summer than during the winter. The large amplitude diurnal cycles in summer vapor d-excess attest to the strong influence of terrestrial moisture sources and atmospheric mixing (Fig. 2c, 4c). The bimodal distributions of d-excess observed during the summer result from positive d-excess values during the day and negative d-excess values at night, which may reflect the loss of leaf water enrichment and exchange with ambient atmospheric vapor overnight (Fig. 7d,e). More exchange of water vapor between the atmosphere and the land surface through ET would progressively overprint the original attributes of an air parcel over the continent, both along its transport to and at the CDFS (Fig. 8,9). This is consistent with the results of our moisture source attribution using back trajectories with a Lagrangian tracer, which indicates the primary advected source of vapor to the CDFS is from land ET in both seasons (Fig. 9). As a result, vapor d-excess is unlikely to preserve the characteristics of the oceanic source of vapor in highly continental settings. Our analysis is consistent with a growing number of studies that have also shown strong variability in vapor d-excess on diurnal timescales (Aemisegger et al., 2014; Lai & Ehleringer, 2010; Parkes et al., 2017; Simonin et al., 2014; Welp et al., 2012).

The relationship between remote RH and d-excess appears stronger in winter than summer (Fig. 10a-f). No consistent relationships are observed between oceanic RH and CDFS d-excess (Fig. 10a,c), and inconsistent but noisy relationships are observed between land ET RH and CDFS d-excess (Fig. 10d,f). These trends suggest a seasonal modulation of the impact of remote versus local conditions on vapor isotope ratios. Summer d-excess values respond most strongly to local RH values, while winter d-excess values show comparable responses to changes in local or remotely-diagnosed land RH (Fig. 10e,h). This suggests a greater balance between local and remote sources of vapor to the CDFS in the winter.

Our results, along with previous studies (e.g., Aemisegger et al., 2014; Griffis et al., 2016; Welp et al., 2012), suggest that long-term isotopic monitoring of water inputs and losses to a region can reliably document the factors contributing to hydrologic variability and change. As vapor isotope measurements become more widespread through efforts such as the National Ecologic Observatory Network, changes in the relative contributions of remote moisture transport through meso-to-synoptic scale weather patterns compared to the local ET flux can be constrained with isotope tracers. Model studies (J.-E. Lee et al., 2012; Risi et al., 2013; Skinner et al., 2017; Swann et al., 2012) and satellite data (Spracklen et al., 2012) suggest that transpiration both can trigger precipitation and minimize the risk of extreme hydroclimatic events such as droughts and floods. Therefore, long-term monitoring may also be useful in assessing changes in the local ET flux relative to the remotely advected vapor flux.

5 Conclusions

Measurements of near-surface water vapor isotopic composition and local meteorology in a deep mountain valley in northwestern Wyoming show substantial seasonal changes in vapor $\delta^{18}O$ and $\delta^{2}H$ and relationships between local conditions, large-scale moisture advection, and patterns of land-atmosphere water exchange. The largest local meteorological factor influencing vapor isotope ratios is specific humidity. As a result, summer vapor is less depleted in heavy isotopologues than winter vapor. Links between local vapor isotope ratios and large-scale moisture sources are identified for both seasons, though conditions at the CDFS cannot be mapped uniquely back to a particular source region due to continued evaporation and precipitation over the continent that progressively replace vapor derived from oceanic evaporative sources with vapor derived from continental ET. With the additional observation that variability in humidity and vapor isotope ratios at the CDFS are primarily driven by air-mass mixing processes, CDFS isotope ratios are consistent with the mixing of distinct vapor masses that have undergone different degrees of condensation, or the addition of surface ET fluxes over the continent. We observe a strong diurnal cycle in vapor d-excess in the summer that is absent in the winter. The most likely explanation for this relationship is that local surface water fluxes, such as ET, are stronger during the summer and dampen the characteristics of advected humidity. In contrast, during the winter, our analysis suggests a more balanced influence by local and remote moisture sources on CDFS vapor isotope ratios. As near-surface stable water vapor

isotopes reflect both local and remote processes, continued measurements will be critical to understand processes driving continental hydrologic variability and change.

6 Acknowledgments

RPF received support from NSF Graduate Research Fellowship 2011094378, a Geological Society of America Graduate Student Grant, and a Turner Award (University of Michigan (UM) Department of Earth and Environmental Sciences). CJP received support from the UM Associate Professor Support Fund and NSF Tectonics Grant F026336. AMM received support from NSF Hydrological Sciences grant 1521238, the Ohio State University Presidential Fellowship and a P.E.O. Scholar Award. Isotope and meteorological data are available on the Open Science Framework (http://osf.io/md7ws). HYSPLIT and wind field input data are available from the NOAA Air Resources Laboratory (http://ready.arl.noaa.gov/HYSPLIT.php).

7 References

Aemisegger, F., Sturm, P., Graf, P., Sodemann, H., Pfahl, S., Knohl, A., & Wernli, H. (2012). Measuring variations of δ 18O and δ 2H in atmospheric water vapour using two commercial laser-based spectrometers: An instrument characterisation study. *Atmospheric Measurement Techniques*, *5*(7), 1491–1511. https://doi.org/10.5194/amt-5-1491-2012

Aemisegger, F., Pfahl, S., Sodemann, H., Lehner, I., Seneviratne, S. I., & Wernli, H. (2014). Deuterium excess as a proxy for continental moisture recycling and plant transpiration. *Atmospheric Chemistry and Physics*, *14*(8), 4029–4054. https://doi.org/10.5194/acp-14-4029-2014

Aemisegger, F., Spiegel, J. K., Pfahl, S., Sodemann, H., Eugster, W., & Wernli, H. (2015). Isotope meteorology of cold front passages: A case study combining observations and modeling. *Geophysical Research Letters*, *42*(13), 5652–5660. https://doi.org/10.1002/2015GL063988

Bailey, A., Toohey, D., & Noone, D. (2013). Characterizing moisture exchange between the Hawaiian convective boundary layer and free troposphere using stable isotopes in water.

Journal of Geophysical Research Atmospheres, *118*(15), 8208–8221. https://doi.org/10.1002/jgrd.50639

Bailey, A., Nusbaumer, J., & Noone, D. C. (2015). Precipitation efficiency derived from isotope ratios in water vapor distiguishes dynamical and microphysical influences on subtropical atmospheric constituents. *Journal of Geophysical Research Atmospheres*, 9119–9137. https://doi.org/10.1002/2015JD023403.Received

Benetti, M., Reverdin, G., Pierre, C., Merlivat, L., Risi, C., Steen-larsen, H. C., & Vimeux, F. (2014). Deuterium excess in marine water vapor: Dependency on relative humidity and surface wind speed during evaporation, 584–593. https://doi.org/10.1002/2013JD020535.Received

Berkelhammer, M., Hu, J., Bailey, A., Noone, D. C., Still, C. J., Barnard, H., … Turnipseed, A. (2013). The nocturnal water cycle in an open-canopy forest. *Journal of Geophysical Research Atmospheres*, *118*(17), 10225–10242. https://doi.org/10.1002/jgrd.50701

Bowen, G. J., & Good, S. P. (2015). Incorporating water isoscapes in hydrological and water resource investigations. *Wiley Interdisciplinary Reviews: Water*, *2*(2), 107–119. https://doi.org/10.1002/wat2.1069

Brown, D., Worden, J., & Noone, D. (2008). Comparison of atmospheric hydrology over convective continental regions using water vapor isotope measurements from space. *Journal of Geophysical Research Atmospheres*, *113*(15), 1–17. https://doi.org/10.1029/2007JD009676

Brunel, J. P., Simpson, H. J., Herczeg, A. L., Whitehead, R., & Walker, G. R. (1992). Stable isotope composition of water vapor as an indicator of transpiration fluxes from rice crops. *Water Resources Research*, *28*(5), 1407–1416. https://doi.org/10.1029/91WR03148

Cappa, C. D., Hendricks, M. B., DePaolo, D. J., & Cohen, R. C. (2003). Isotopic fractionation of water during evaporation. *Journal of Geophysical Research*, *108*(D16), 4525. https://doi.org/10.1029/2003JD003597

Coplen, T. B. (1996). New guidelines for reporting stable hydrogen, carbon, and oxygen isotope-ratio data. *Geochimica et Cosmochimica Acta*, *60*(17), 3359–3360. https://doi.org/10.1016/0016-7037(96)00263-3

Craig, H. (1961). Isotopic variations in meteoric waters. *Science*, *133*(3465), 1702–1703.

Craig, H., & Gordon, L. I. (1965). *Deuterium and oxygen 18 variations in the ocean and the marine atmosphere*. *Stable Isotopes in Oceanographic Studies and Paleotemperatures*. Retrieved from http://yncenter.sites.yale.edu/sites/default/files/shen_jing_jan_2013.pdf

Dansgaard, W. (1964). Stable isotopes in precipitation. *Tellus*, *16*(4), 436–468. https://doi.org/10.3402/tellusa.v16i4.8993

Despain, D. G. (1987). The two climates of Yellowstone National Park. *Proceedings of the Montana Academy of Science*, *47*, 11–20.

Dessler, A. E., & Sherwood, S. C. (2003). A model of HDO in the tropical tropopause layer. *Atmospheric Chemistry and Physics*, *3*, 2173–2181. https://doi.org/10.5194/acpd-3-4489-2003

Diffenbaugh, N. S., Swain, D. L., & Touma, D. (2015). Anthropogenic warming has increased drought risk in California. *Proceedings of the National Academy of Sciences*, *112*(13), 3931–3936. https://doi.org/10.1073/pnas.1422385112

Draxler, R. R., & Hess, G. D. (1998). An Overview of the HYSPLIT_4 Modelling System for Trajectories, Dispersion, and Deposition. *Australian Meteorological Magazine*, *47*(January), 295–308.

Ehhalt, D. H., Rohrer, F., & Fried, A. (2005). Vertical profiles of HDO/H2O in the troposphere. *Journal of Geophysical Research*, *110*, 1–13. https://doi.org/10.1029/2004JD005569

van der Ent, R. J., Savenije, H. H. G., Schaefli, B., & Steele-Dunne, S. C. (2010). Origin and fate of atmospheric moisture over continents. *Water Resources Research*, *46*(9), 1–12. https://doi.org/10.1029/2010WR009127

Ficklin, D. L., & Novick, K. A. (2017). Historic and projected changes in vapor pressure deficit suggest a continental-scale drying of the United States atmosphere. *Journal of Geophysical Research Atmospheres*, *122*, 2061–2079. https://doi.org/10.1002/2016JD025855

Fiorella, R. P., Bares, R., Lin, J. C., Ehleringer, J. R., & Bowen, G. J. (2018). Detection and variability of combustion-derived vapor in an urban basin. *Atmospheric Chemistry and Physics Discussions*.

Friedman, I., Harris, J. M., Smith, G. I., & Johnson, C. A. (2002). Stable isotope composition of waters in the Great Basin, United States 1. Air-mass trajectories. *Journal of Geophysical Research Atmospheres*, *107*(19), 1–14. https://doi.org/10.1029/2001JD000565

Galewsky, J. (2009). Orographic precipitation isotopic ratios in stratified atmospheric flows: Implications for paleoelevation studies. *Geology*, *37*(9), 791–794. https://doi.org/10.1130/G30008A.1

Galewsky, J., & Hurley, J. V. (2010). An advection-condensation model for subtropical water vapor isotopic ratios. *Journal of Geophysical Research Atmospheres*, *115*(16), 1–10. https://doi.org/10.1029/2009JD013651

Galewsky, J., & Samuels-Crow, K. (2015). Summertime moisture transport to the southern South American Altiplano: Constraints from in situ measurements of water vapor isotopic composition. *Journal of Climate*, *28*(7), 2635–2649. https://doi.org/10.1175/JCLI-D-14-00511.1

Galewsky, J., Steen-Larsen, H. C., Field, R. D., Worden, J., Risi, C., & Schneider, M. (2016). Stable isotopes in atmospheric water vapor and applications to the hydrologic cycle. *Reviews of Geophysics*, *54*, 809–865. https://doi.org/10.1002/2015RG000512

Galewsky, J., Rella, C., Sharp, Z., Samuels, K., & Ward, D. (2011). Surface measurements of upper tropospheric water vapor isotopic composition on the Chajnantor Plateau, Chile. *Geophysical Research Letters*, *38*(17), 1–5. https://doi.org/10.1029/2011GL048557

Gat, J. R. (1996). Oxygen and Hydrogen Isotopes in the Hydrologic Cycle. *Annual Review of Earth and Planetary Sciences*, *24*(1), 225–262. https://doi.org/10.1146/annurev.earth.24.1.225

Gedzelman, S. D. (1988). Deuterium in water vapor above the atmospheric boundary layer.

Tellus B, *40*(2), 134–147. https://doi.org/10.1111/j.1600-0889.1988.tb00217.x

Good, S. P., Soderberg, K., Guan, K., King, E. G., Scanlon, T. M., & Caylor, K. K. (2014). d2H isotopic flux partitioning of evapotranspiration over a grass field following a water pulse and subsequent dry down. *Water Resources Research*, *50*, 1410–1432. https://doi.org/10.1002/2013WR01433

Griffis, T. J., Wood, J. D., Baker, J. M., Lee, X., Xiao, K., Chen, Z., … Nieber, J. (2016). Investigating the source , transport , and isotope composition of water vapor in the planetary boundary layer, 5139–5157. https://doi.org/10.5194/acp-16-5139-2016

Hayes, J. M. (1982). Fractionation, et al.; an introduction to isotopic measurements and terminology. *Spectra*, *8*(4), 3–8.

He, H., & Smith, R. B. (1999). Stable isotope composition of water vapor in the atmospheric boundary layer above the forests of New England. *Journal of Geophysical Research: Atmospheres*, *104*(D9), 11657–11673. https://doi.org/10.1029/1999JD900080

Helliker, B. R., Roden, J. S., Cook, C., & Ehleringer, J. R. (2002). A rapid and precise method for sampling and determining the oxygen isotope ratio of atmospheric water vapor. *Rapid Communications in Mass Spectrometry*, *16*(10), 929–932. https://doi.org/10.1002/rcm.659

Horita, J., & Wesolowski, D. J. (1994). Liquid-vapor fractionation of oxygen and hydrogen isotopes of water from the freezing to the critical temperature. *Geochimica et Cosmochimica Acta*, *58*(16), 3425–3437. https://doi.org/10.1016/0016-7037(94)90096-5

Horton, D. E., Johnson, N. C., Singh, D., Swain, D. L., Rajaratnam, B., & Diffenbaugh, N. S. (2015). Contribution of changes in atmospheric circulation patterns to extreme temperature trends. *Nature*, *522*(7557), 465–469. https://doi.org/10.1038/nature14550

Houghton, J. G. (1969). Weather types and the associated rainfall patterns. In *Charateristics of Rainfall in the Great Basin* (pp. 13–89). Reno, NV: Desert Research Institute.

Jouzel, J. (1986). Isotopes in cloud physics: Multi step and multi stage processes. In *The Terrestrial Environment B* (pp. 61–112).

Jouzel, J., Merlivat, L., & Lorius, C. (1982). Deuterium excess in an East Antarctic ice core suggests higher relative humidity at the oceanic surface during the last glacial maximum. *Nature*, *299*, 688–691.

Kalnay, E., Kanamitsu, M., Kistler, R., Collins, W., Deaven, D., Gandin, L., … Joseph, D. (1996). The NCEP/NCAR 40-year reanalysis project. *Bulletin of the American Meteorological Society*, *77*(3), 437–471. https://doi.org/10.1175/1520-0477(1996)077<0437:TNYRP>2.0.CO;2

Keeling, C. D. (1958). The concentration and isotopic abundances of atmospheric carbon dixoide in rural areas. *Geochimica et Cosmochimica Acta*, *13*, 322–334.

Keeling, C. D. (1961). The concentration and isotopic Abundances of Carbon Dioxide in rural and marine air. *Geochimica et Cosmochimica Acta*, *24*, 277–298.

Lai, C. T., & Ehleringer, J. R. (2010). Deuterium excess reveals diurnal sources of water vapor in forest air. *Oecologia*, *165*(1), 213–223. https://doi.org/10.1007/s00442-010-1721-2

Lechler, A. R., & Galewsky, J. (2013). Refining paleoaltimetry reconstructions of the Sierra

Nevada: California, using air parcel trajectories. *Geology*, *41*(2), 259–262. https://doi.org/10.1130/G33553.1

Lee, J.-E., & Fung, I. Y. (2008). "Amount effect" of water isotopes and quantitative analysis of post-condensation processes. *Hydrological Processes*, *22*, 1–8. https://doi.org/10.1002/hyp.6637

Lee, J.-E., Lintner, B. R., Neelin, J. D., Jiang, X., Gentine, P., Boyce, C. K., … Worden, J. (2012). Reduction of tropical land region precipitation variability via transpiration. *Geophysical Research Letters*, *39*(19), 1–6. https://doi.org/10.1029/2012GL053417

Lee, X., Smith, R., & Williams, J. (2006). Water vapour 18O/16O isotope ratio in surface air in New England, USA. *Tellus, Series B: Chemical and Physical Meteorology*, *58*(4), 293–304. https://doi.org/10.1111/j.1600-0889.2006.00191.x

Liu, B., Xu, M., Henderson, M., & Gong, W. (2004). A spatial analysis of pan evaporation trends in China, 1955-2000. *Journal of Geophysical Research D: Atmospheres*, *109*(15), 1–9. https://doi.org/10.1029/2004JD004511

Luz, B., Barkan, E., Yam, R., & Shemesh, A. (2009). Fractionation of oxygen and hydrogen isotopes in evaporating water. *Geochimica et Cosmochimica Acta*, *73*(22), 6697–6703. https://doi.org/10.1016/j.gca.2009.08.008

Majoube, M. (1971). Fractionnement en oxygene-18 et en deuterium entre l'eau et sa vapeur. *Journal de Chimie et Physique*, *58*, 1423–1436.

Merlivat, L., & Jouzel, J. (1979). Global climatic interpretation of the Deuterium-Oyxgen 18 relationship for precipitation. *Journal of Geophysical Research*, *84*(C8), 5029–5033.

Mesinger, F., DiMego, G., Kalnay, E., Mitchell, K., Shafran, P. C., Ebisuzaki, W., … Shi, W. (2006). North American regional reanalysis. *Bulletin of the American Meteorological Society*, *87*(3), 343–360. https://doi.org/10.1175/BAMS-87-3-343

Miller, J. B., & Tans, P. P. (2003). Calculating isotopic fractionation from atmospheric measurements at various scales. *Tellus, Series B: Chemical and Physical Meteorology*, *55*(2), 207–214. https://doi.org/10.1034/j.1600-0889.2003.00020.x

Noone, D. C. (2012). Pairing measurements of the water vapor isotope ratio with humidity to deduce atmospheric moistening and dehydration in the tropical midtroposphere. *Journal of Climate*, *25*(13), 4476–4494. https://doi.org/10.1175/JCLI-D-11-00582.1

Noone, D. C., Risi, C., Bailey, A., Berkelhammer, M., Brown, D. P., Buenning, N., … Wolfe, D. (2013). Determining water sources in the boundary layer from tall tower profiles of water vapor and surface water isotope ratios after a snowstorm in Colorado. *Atmospheric Chemistry and Physics*, *13*(3), 1607–1623. https://doi.org/10.5194/acp-13-1607-2013

Noone, D. C., Galewsky, J., Sharp, Z. D., Worden, J., Barnes, J., Baer, D., … Wright, J. S. (2011). Properties of air mass mixing and humidity in the subtropics from measurements of the D/H isotope ratio of water vapor at the Mauna Loa Observatory. *Journal of Geophysical Research Atmospheres*, *116*(22), 1–18. https://doi.org/10.1029/2011JD015773

Novick, K. A., Ficklin, D. L., Stoy, P. C., Williams, C. A., Bohrer, G., Oishi, A. C., … Phillips, R. P. (2016). The increasing importance of atmospheric demand for ecosystem water and

carbon fluxes. *Nature Climate Change*, *6*(11), 1023–1027. https://doi.org/10.1038/nclimate3114

Parkes, S. D., McCabe, M. F., Griffiths, A. D., Wang, L., Chambers, S., Ershadi, A., … Element, A. (2017). Response of water vapour D-excess to land-atmosphere interactions in a semi-arid environment. *Hydrology and Earth System Sciences*, *21*(1), 533–548. https://doi.org/10.5194/hess-21-533-2017

Pataki, D. E., Ehleringer, J. R., Flanagan, L. B., Yakir, D., Bowling, D. R., Still, C. J., … Berry, J. A. (2003). The application and interpretation of Keeling plots in terrestrial carbon cycle research. *Global Biogeochemical Cycles*, *17*(1), n/a-n/a. https://doi.org/10.1029/2001GB001850

Pfahl, S., & Sodemann, H. (2014). What controls deuterium excess in global precipitation? *Climate of the Past*, *10*(2), 771–781. https://doi.org/10.5194/cp-10-771-2014

Pfahl, S., & Wernli, H. (2008). Air parcel trajectory analysis of stable isotopes in water vapor in the eastern Mediterranean. *Journal of Geophysical Research Atmospheres*, *113*(20), 1–16. https://doi.org/10.1029/2008JD009839

Risi, C., Bony, S., & Vimeux, F. (2008). Influence of convective processes on the isotopic composition ($\delta^{18}O$ and δD) of precipitation and water vapor in the tropics: 2. Physical interpretation of the amount effect. *Journal of Geophysical Research Atmospheres*, *113*(19), 1–12. https://doi.org/10.1029/2008JD009943

Risi, C., Noone, D., Frankenberg, C., & Worden, J. (2013). Role of continental recycling in intraseasonal variations of continental moisture as deduced from model simulations and water vapor isotopic measurements. *Water Resources Research*, *49*(7), 4136–4156. https://doi.org/10.1002/wrcr.20312

Roderick, M. L., & Farquhar, G. D. (2002). The Cause of Decreased Pan Evaporation over the Past 50 Years. *Science*, *298*(5597), 1407–1410. https://doi.org/10.1126/science.1075390

Roderick, M. L., Rotstayn, L. D., Farquhar, G. D., & Hobbins, M. T. (2007). On the attribution of changing pan evaporation. *Geophysical Research Letters*, *34*(17), 1–6. https://doi.org/10.1029/2007GL031166

Rozanski, K., Araguás-Araguás, L., & Gonfiantini, R. (1993). Isotopic Patterns in Modern Global Precipitation. In P. K. Swart, K. C. Lohmann, J. McKenzie, & S. M. Savin (Eds.), *Climate Change in Continental Isotopic Records* (pp. 1–36). Washington, DC: American Geophysical Union.

Rozanski, K., & Sonntag, C. (1982). Vertical distribution of deuterium in atmospheric water vapour. *Tellus*, *34*(2), 135–141. https://doi.org/10.1111/j.2153-3490.1982.tb01800.x

Samuels-Crow, K. E., Galewsky, J., Hardy, D. R., Sharp, Z. D., Worden, J., & Braun, C. (2014). Upwind convective influences on the isotopic composition of atmospheric water vapor over the tropical Andes. *Journal Of Geophysical Research-Atmospheres*, *119*, 7051–7063. https://doi.org/10.1002/2014JD021487.Received

Schmidt, M., Maseyk, K., Lett, C., Biron, P., Richard, P., Bariac, T., & Seibt, U. (2010). Concentration effects on laser-based d18O and d2H measurements and implications for the

calibration of vapour measurements with liquid standards. *Rapid Communications in Mass Spectrometry*, *24*, 3553–3561. https://doi.org/10.1002/rcm.4813

Seneviratne, S. I., Donat, M. G., Mueller, B., & Alexander, L. V. (2014). No pause in the increase of hot temperature extremes. *Nature Climate Change*, *4*(3), 161–163. https://doi.org/10.1038/nclimate2145

Seneviratne, S. I., Corti, T., Davin, E. L., Hirschi, M., Jaeger, E. B., Lehner, I., … Teuling, A. J. (2010). Investigating soil moisture-climate interactions in a changing climate: A review. *Earth-Science Reviews*, *99*(3–4), 125–161. https://doi.org/10.1016/j.earscirev.2010.02.004

Simonin, K. A., Roddy, A. B., Link, P., Apodaca, R., Tu, K. P., Hu, J., … Barbour, M. M. (2013). Isotopic composition of transpiration and rates of change in leaf water isotopologue storage in response to environmental variables. *Plant, Cell and Environment*, *36*(12), 2190–2206. https://doi.org/10.1111/pce.12129

Simonin, K. A., Link, P., Rempe, D., Miller, S., Oshun, J., Bode, C., … Dawson, T. E. (2014). Vegetation induced changes in the stable isotope composition of near surface humidity. *Ecohydrology*, *7*(3), 936–949. https://doi.org/10.1002/eco.1420

Singh, D., Swain, D. L., Mankin, J. S., Horton, D. E., Thomas, L. N., Rajaratnam, B., & Diffenbaugh, N. S. (2016). Recent amplification of the North American winter temperature dipole. *Journal of Geophysical Research Atmospheres*, 1411–1428. https://doi.org/10.1002/2016JD025116

Skinner, C. B., Poulsen, C. J., Chadwick, R., Diffenbaugh, N. S., & Fiorella, R. P. (2017). The role of plant CO2 physiological forcing in shaping future daily-scale precipitation. *Journal of Climate*, *30*(7), 2319–2340. https://doi.org/10.1175/JCLI-D-16-0603.1

Sodemann, H., Schwierz, C., & Wernli, H. (2008). Interannual variability of Greenland winter precipitation sources: Lagrangian moisture diagnostic and North Atlantic Oscillation influence. *Journal of Geophysical Research Atmospheres*, *113*(3), 1–17. https://doi.org/10.1029/2007JD008503

Sodemann, H., Aemisegger, F., Pfahl, S., Bitter, M., Corsmeier, U., Feuerle, T., … Wernli, H. (2017). The stable isotopic composition of water vapour above Corsica during the HyMeX SOP1 campaign: Insight into vertical mixing processes from lower-tropospheric survey flights. *Atmospheric Chemistry and Physics*, *17*(9), 6125–6151. https://doi.org/10.5194/acp-17-6125-2017

Spracklen, D. V., Arnold, S. R., & Taylor, C. M. (2012). Observations of increased tropical rainfall preceded by air passage over forests. *Nature*, *489*(7415), 282–285. https://doi.org/10.1038/nature11390

Steen-Larsen, H. C., Sveinbjörnsdottir, A. E., Jonsson, T., Ritter, F., Bonne, J., Sodemann, H., … Vinther, B. M. (2015). Moisture sources and synoptic to seasonal variability of North Atlantic water vapor isotopic composition. *Journal Geophysical Research Atmospheres*, *120*, 5757–5774. https://doi.org/10.1002/2015JD023234.Received

Stewart, M. K. (1975). Stable isotope fractionation due to evaporation and isotopic exchange of falling waterdrops: Applications to atmospheric processes and evaporation of lakes. *Journal*

of Geophysical Research, *80*(9), 1133. https://doi.org/10.1029/JC080i009p01133

Sturm, P., & Knohl, A. (2009). Water vapor δ2H and δ18O measurements using off-axis integrated cavity output spectroscopy. *Atmospheric Measurement Techniques*, *2*(4), 2055–2085. https://doi.org/10.5194/amtd-2-2055-2009

Swann, A. L. S., Fung, I. Y., & Chiang, J. C. H. (2012). Mid-latitude afforestation shifts general circulation and tropical precipitation. *Proceedings of the National Academy of Sciences*, *109*(3), 712–716. https://doi.org/10.1073/pnas.1116706108

Tremoy, G., Vimeux, F., Cattani, O., Mayaki, S., Souley, I., & Favreau, G. (2011). Measurements of water vapor isotope ratios with wavelength-scanned cavity ring-down spectroscopy technology: New insights and important caveats for deuterium excess measurements in tropical areas in comparison with isotope-ratio mass spectrometry. *Rapid Communications in Mass Spectrometry*, *25*(23), 3469–3480. https://doi.org/10.1002/rcm.5252

Trenberth, K. E., Fasullo, J., Smith, L., Qian, T., & Dai, A. (2006). Estimates of the Global Water Budget and Its Annual Cycle Using Observational and Model Data. *Journal of Hydrometeorology - Special Section*, *8*, 758–769. https://doi.org/10.1175/JHM600.1

Uemura, R., Matsui, Y., Yoshimura, K., Motoyama, H., & Yoshida, N. (2008). Evidence of deuterium excess in water vapor as an indicator of ocean surface conditions. *Journal of Geophysical Research Atmospheres*, *113*(19), 1–10. https://doi.org/10.1029/2008JD010209

Wei, Z., Yoshimura, K., Okazaki, A., Ono, K., Kim, W., Yokoi, M., & Lai, C. T. (2016). Understanding the variability of water isotopologues in near-surface atmospheric moisture over a humid subtropical rice paddy in Tsukuba, Japan. *Journal of Hydrology*, *533*, 91–102. https://doi.org/10.1016/j.jhydrol.2015.11.044

Welp, L. R., Lee, X., Kim, K., Griffis, T. J., Billmark, K. A., & Baker, J. M. (2008). d18O of water vapour, evapotranspiration and the sites of leaf water evaporation in a soybean canopy. *Plant, Cell and Environment*, *31*(9), 1214–1228. https://doi.org/10.1111/j.1365-3040.2008.01826.x

Welp, L. R., Lee, X., Griffis, T. J., Wen, X. F., Xiao, W., Li, S., … Huang, J. (2012). A meta-analysis of water vapor deuterium-excess in the midlatitude atmospheric surface layer. *Global Biogeochemical Cycles*, *26*(3), 1–12. https://doi.org/10.1029/2011GB004246

Wen, X. F., Lee, X., Sun, X. M., Wang, J. L., Hu, Z. M., Li, S. G., & Yu, G. R. (2012). Dew water isotopic ratios and their relationships to ecosystem water pools and fluxes in a cropland and a grassland in China. *Oecologia*, *168*(2), 549–561. https://doi.org/10.1007/s00442-011-2091-0

White, J. W. C., & Gedzelman, S. D. (1984). The isotopic composition of atmospheric water vapor and the concurrent meteorological conditions. *Journal of Geophysical Research*, *89*(03), 4937–4939. Retrieved from http://www.agu.org/pubs/crossref/1984/JD089iD03p04937.shtml

Whiteman, C. D. (1982). Breakup of Temperature Inversions in Deep Mountain Valleys: Part I. Observations. *Journal of Applied Meteorology*. https://doi.org/10.1175/1520-

0450(1983)022<1314:COOTII>2.0.CO;2
Whiteman, C. D., Pospichal, B., Eisenbach, S., Weihs, P., Clements, C. B., Steinacker, R., … Dorninger, M. (2004). Inversion Breakup in Small Rocky Mountain and Alpine Basins. *Journal of Applied Meteorology*, *43*, 1069–1082. https://doi.org/10.1175/1520-0450(2004)043<1069:IBISRM>2.0.CO;2
Whiteman, C. D., Bian, X., & Zhong, S. (1999). Wintertime evolution of the temperature inversion in the Colorado Plateau Basin. *Journal of Applied Meteorology*, *38*(8), 1103–1117. https://doi.org/10.1175/1520-0450(1999)038<1103:WEOTTI>2.0.CO;2
Yu, L., & Weller, R. A. (2007). Objectively Analyzed Air-Sea Heat Fluxes for the Global Ice-Free Oceans (1981-2005). *Bulletin of the American Meteorological Society*, (April), 527–539. https://doi.org/10.1175/BAMS-88-4-527

Tables

Table 1. Mean Isotopic Compositions and Meteorological Conditions

Measurement period	$\delta^{18}O$ (‰ VSMOW)	$\delta^{2}H$ (‰ VSMOW)	d-excess (‰ VSMOW)	2-m *q* (g kg^{-1})	2-m T (°C)	Total precipitation (mm)
Jun 13-Sep 3, 2012	-19.8	-155.4	3.3	6.2	17.4	42.3
Jan 13-Feb 5, 2013	-33.5	-251.5	16.8	1.9	-10.3	N/A
Jul 2-Jul 18, 2014	-20.5	-164.2	0.0	7.5	17.2	16.2

Table 2. Correspondence between $\delta^{18}O$ Measurements and Isotopic Box Model Results

Warm ocean source, 25°C, 90% RH			
	Summer 2012	Winter 2013	Summer 2014
Too moist for all models	0.0%	0.0%	0.0%
Too depleted in heavy isotopes for Rayleigh	33.7%	30.9%	83.5%
Between Rayleigh and closed condensation	62.1%	52.2%	16.3%
Between closed condensation and mixing	4.1%	16.8%	0.2%
Too enriched in heavy isotopes for mixing	0.0%	0.1%	0.0%
Cool ocean source, 10°C, 90% RH			
	Summer 2012	Winter 2013	Summer 2014
Too moist for all models	34.1%	0.0%	60.8%
Too depleted in heavy isotopes for Rayleigh	62.9%	52.0%	40.1%
Between Rayleigh and closed condensation	0.9%	32.1%	0.0%
Between closed condensation and mixing	0.0%	15.7%	0.0%
Too enriched in heavy isotopes for mixing	0.0%	0.2%	0.0%

Table 3. Percentage of CDFS record associated with different atmospheric processes

Process	Summer 2012	Winter 2013	Summer 2014
$\delta^{18}O$			
Air mass mixing	76.6%	96.2%	85.6%
Condensation	2.7%	0.0%	0.8%

Neither dominant	20.7%	3.8%	13.7%
δ^2H			
Air mass mixing	80.3%	96.0%	95.1%
Condensation	2.1%	0.0%	0.0%
Neither dominant	17.6%	4.0%	4.9%

Table 4. Percentage of CDFS record associated with distinct air source regions

Wind Field Source	North Pacific	Northern Continental	High Sierra	Subtropical Pacific	Southern Continental
Summer 2012					
NARR	53.0	5.8	0.3	40.5	0.3
GDAS	47.6	4.6	3.4	42.4	2.1
NCEP	60.1	3.0	3.7	31.4	1.8
Winter 2013					
NARR	81.7	6.5	1.1	10.8	0.0
GDAS	74.2	8.6	0.0	17.2	0.0
NCEP	77.4	8.6	1.1	12.9	0.0
Summer 2014					
NARR	78.1	12.5	0.0	9.4	0.0
GDAS	70.3	17.2	0.0	12.5	0.0
NCEP	81.3	18.8	0.0	0.0	0.0

Table 5. Average CDFS Vapor Characteristics Associated with Air Source Regions Identified from NCEP, GDAS, NARR Wind Field Sources

Source Pathway	Mean q (mmol mol^{-1})			Mean $\delta^{18}O$ (‰VSMOW)			Mean d (‰ VSMOW)		
	NCEP	GDAS	NARR	NCEP	GDAS	NARR	NCEP	GDAS	NARR
Summer 2012									
N. Pacific	9.1±3.3	8.7±2.6	8.9±2.9	-21.0±2.7	-21.2±2.4	-21.1±2.6	3.7±11.5	2.9±11.2	3.8±11.4
N. Continental	8.3±1.3	9.8±2.8	8.9±1.9	-21.5±0.7	-19.8±2.1	-20.3±2.4	-7.0±7.9	1.2±9.8	1.7±9.9
High Sierra	9.5±1.4	9.8±3.8	9.8±0.5	-20.6±1.4	-21.0±3.7	-17.0±0.2	-0.1±9.4	16.3±11.6	-3.5±2.1
Subtropical Pacific	11.5±2.9	11.3±3.4	11.4±3.2	-17.8±2.5	-18.3±3.0	-18.2±2.6	3.3±10.7	3.2±10.9	3.0±10.9
S. Continental	11.5±2.8	11.3±2.5	17.8±0.3	-16.0±1.7	-15.8±1.7	-10.4±0.4	5.1±8.3	2.5±7.8	-4.2±1.1
Winter 2013									
N. Pacific	2.8±1.6	2.9±1.6	2.9±1.7	-33.3±2.9	-33.2±3.0	-33.4±2.9	16.5±3.5	16.4±3.6	16.5±3.6
N. Continental	1.3±0.3	1.3±0.3	1.3±0.3	-37.1±0.9	-37.1±0.9	-37.4±0.7	16.3±2.6	16.3±2.6	16.8±1.8
High Sierra	6.3±0.3	N/A	5.7±0.8	-30.9±0.4	N/A	-33.4±0.4	15.4±0.5	N/A	16.6±0.8
Subtropical Pacific	5.2±1.8	4.6±2.0	5.0±1.8	-33.4±2.1	-33.9±1.7	-33.4±2.0	18.9±2.7	18.7±2.2	19.1±2.5
S. Continental	N/A	N/A	N/A	N/A	N/A	N/A	N/A	N/A	N/A
Summer 2014									
N. Pacific	11.5±3.2	11.4±3.2	11.9±3.3	-20.9±1.5	-20.8±1.6	-20.6±1.6	0.0±12.2	0.0±12.3	0.3±12.0
N. Continental	14.5±2.6	14.8±3.2	14.2±2.9	-18.9±0.9	-18.9±0.8	-19.0±0.7	0.0±7.3	1.7±7.6	1.9±7.3
High Sierra	N/A	N/A	N/A	N/A	N/A	N/A	N/A	N/A	N/A
Subtropical Pacific	N/A	11.8±2.2	10.8±2.5	N/A	-21.1±1.3	-21.5±1.3	N/A	-2.3±10.6	-3.8±10.2
S. Continental	N/A	N/A	N/A	N/A	N/A	N/A	N/A	N/A	N/A

Figure Captions

Figure 1. Location of the Camp Davis field station (CDFS). Topography is indicated by grayscale shading on the map, with lighter shades reflecting higher elevation. The boundaries between the five air source regions are indicated with thick orange lines.

Figure 2. Time series of summer 2012 isotopic and meteorological data (DOY 165-247). (a) Specific humidity, q (2 m, g kg^{-1}), (b) $\delta^{18}O$ (black) and $\delta^{2}H$ (red) (‰VSMOW), (c) d-excess (‰ VSMOW), (d) temperature (2 m, °C), (e) relative humidity (2 m, %), and (f) precipitation amount (mm).

Figure 3. Time series of winter 2013 isotopic and meteorological data (DOY 13-35). (a) Specific humidity, q (2 m, g kg^{-1}), (b) $\delta^{18}O$ (solid black) and $\delta^{2}H$ (dashed blue) (‰ VSMOW), (c) d-excess (‰ VSMOW), (d) temperature (2 m, °C), and (e) relative humidity (2 m, %). CDFS precipitation data not available during the winter as the precipitation gauge was unheated.

Figure 4. Time series of summer 2014 isotopic and meteorological data (DOY 165-247). (a) Specific humidity, q (2 m, g kg^{-1}), (b) $\delta^{18}O$ (black) and $\delta^{2}H$ (red) (‰VSMOW), (c) d-excess (‰ VSMOW), (d) temperature (2 m, °C), (e) relative humidity (2 m, %), and (f) precipitation amount (mm).

Figure 5. The δ^2H vs $\delta^{18}O$ relationship. Summer 2012, winter 2013, and summer 2014 data are shown as light red circles, blue triangles, and dark red squares respectively. The global meteoric water line (GMWL) suggested by (Dansgaard, *1964*) is shown by solid black line. Data from winter 2013 plot in a narrow envelope surrounding the GMWL, while the summer data exhibits a much larger range of variability about the GMWL.

Figure 6. Scatterplots of specific humidity (q, mmol mol^{-1}) vs $\delta^{18}O$ (a) or δ^2H (b) and the product of vapor pressure and isotopic composition ($q\delta$) vs q for $q\delta^{18}O$ (c) and $q\delta^2H$ (d). Summer 2012 data are shown as light red triangles, winter 2013 data as blue dots, and summer 2014 data as dark red triangles. Modeled isotopic ratios of moist air at 100% RH and 25°C mixed with dry continental air is shown as a solid black line, while Rayleigh, closed-system, and "super-Rayleigh" condensation are shown starting from the mixing line at 90% RH as dashed, dotted, and dash-dot lines respectively. Equivalent Rayleigh and closed-system condensation models associated with a cooler ocean source (10°C) are shown as gray lines.

Figure 7. The dependence of the relationship between $\delta^{18}O$ and q (top row; a-c) and the distribution of d-excess (bottom row; d-f) on air source region determined from NARR back-trajectories for summer 2012 (left column, a and d), summer 2014 (middle column, b and e), and winter 2013 (right column, c and f). Isotope box model compositions corresponding to air-mass mixing (solid), closed condensation (dotted), Rayleigh condensation (dashed), and "super-

Rayleigh" condensation (dot-dash) are shown in a-c. Distributions of d-excess (d-f) are split into day (solid) and night (dashed) components.

Figure 8. Moisture contributions to the CDFS (g kg^{-1} km^{-2}) for the Summer 2012 (top), Winter 2013 (middle) and Summer 2014 (bottom) observation periods from the NARR dataset as determined by the Sodemann et al. (2008) Lagrangian tracer. Contributions were aggregated to a 1.0°, weighted by their contribution to humidity at the CDFS, and normalized by the grid cell area. Each season has separate maps for each air source pathway, as well as a composite of all trajectories in the observation period.

Figure 9. Proportion of humidity at CDFS apportioned to within PBL moisture uptakes, above PBL moisture uptakes, and the undeterminable fraction for each back-trajectory data source (top row – NARR; middle row – GDAS; bottom row – NCEP) and season (left column – Summer 2012; middle column – Winter 2013; right column – Summer 2014). Moisture uptakes within the PBL are divided into fractions occurring over land (light green) and ocean (dark green), above PBL uptakes are shown in dark blue. The fraction of moisture that cannot be attributed to a source along the trajectory is shown in light blue.

Figure 10. Relationships between diagnosed remote vapor source relative humidity (a-f) or local relative humidity (g-i) at CDFS and vapor d-excess. Remote vapor source relative humidity

values for the three back-trajectory wind sources corresponding to oceanic evaporation (a-c) and evapotranspiration over land (d-f) are plotted against coeval 24-hour running average d-excess values measured at CDFS. A 24-hour running average was used in (a-f) for CDFS d-excess values to remove the influence of local, diurnal processes. No running average was applied to (g-i) for either d-excess nor relative humidity. Linear fits are plotted with a 95% confidence interval when the fit is significant ($p \leq 0.05$), and the slope and Pearson correlation coefficient are shown for these fits in an inset.

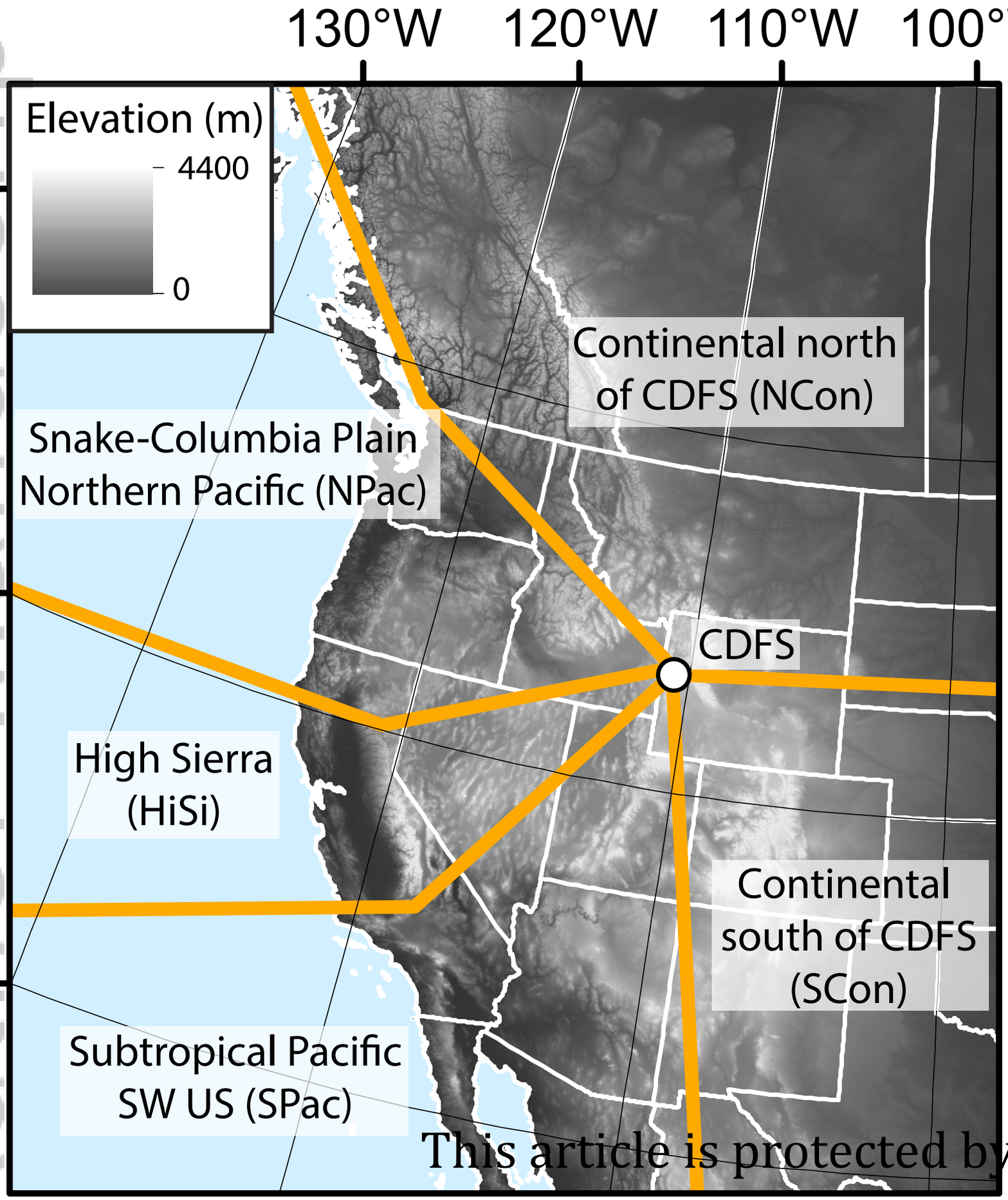

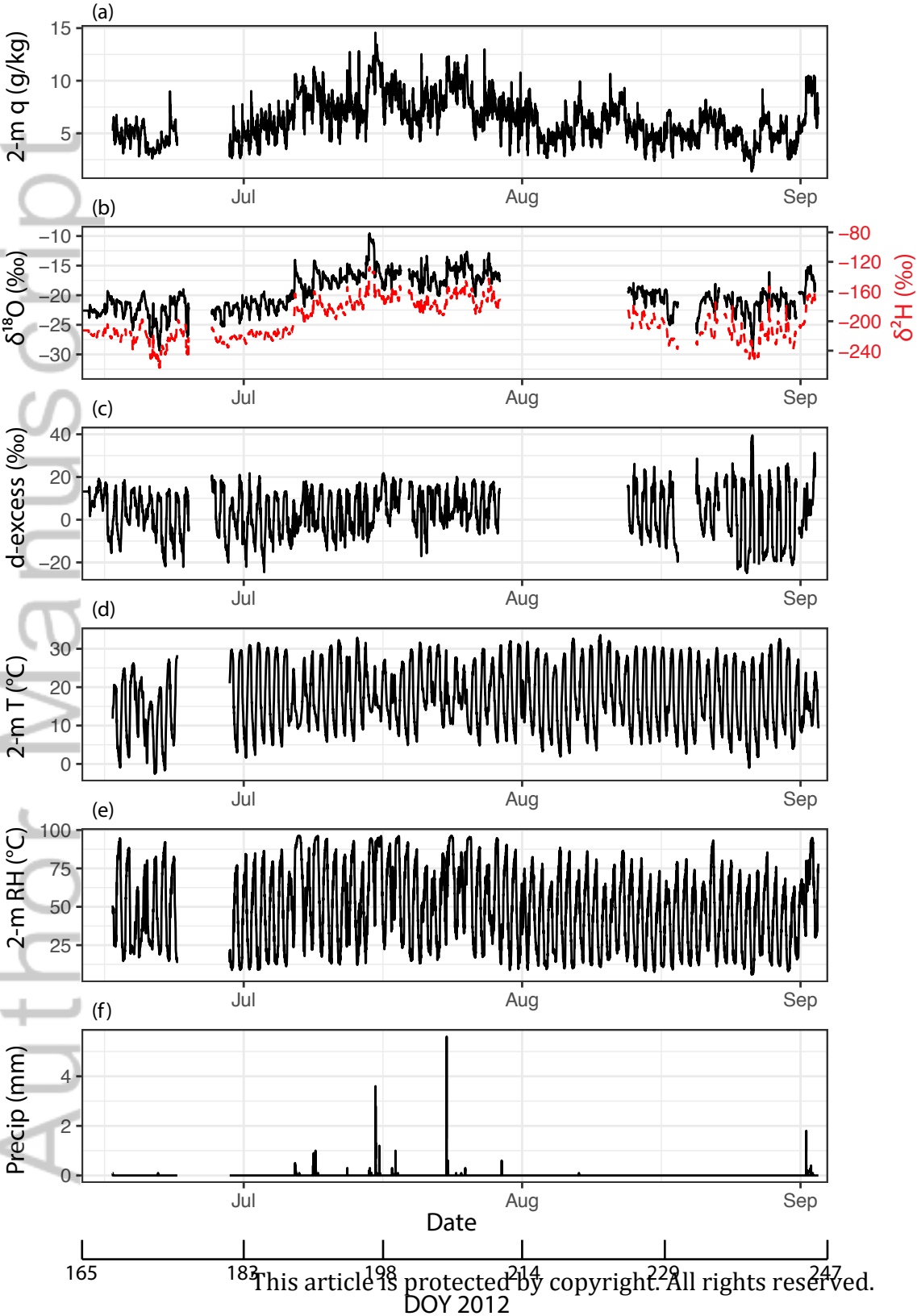

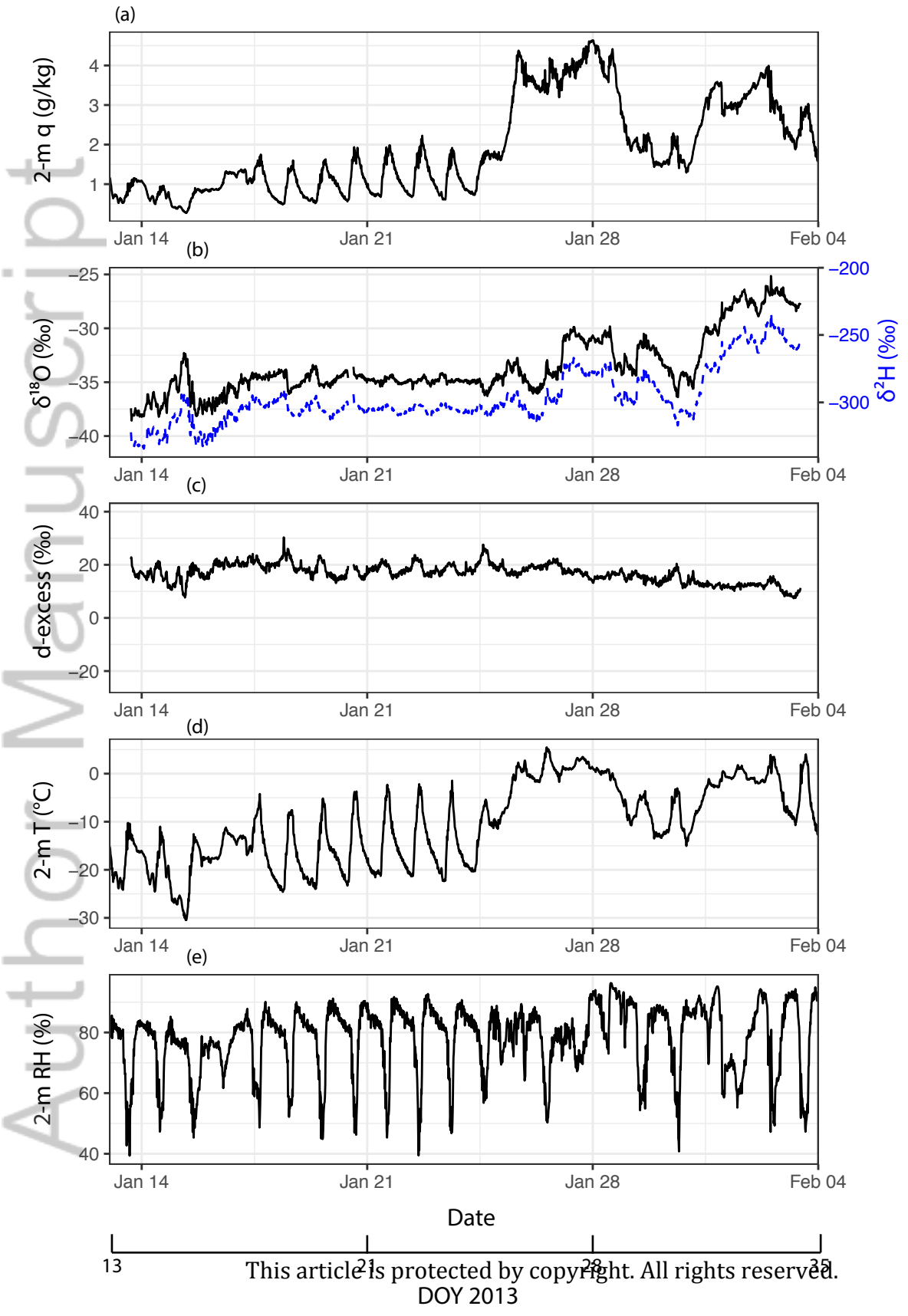

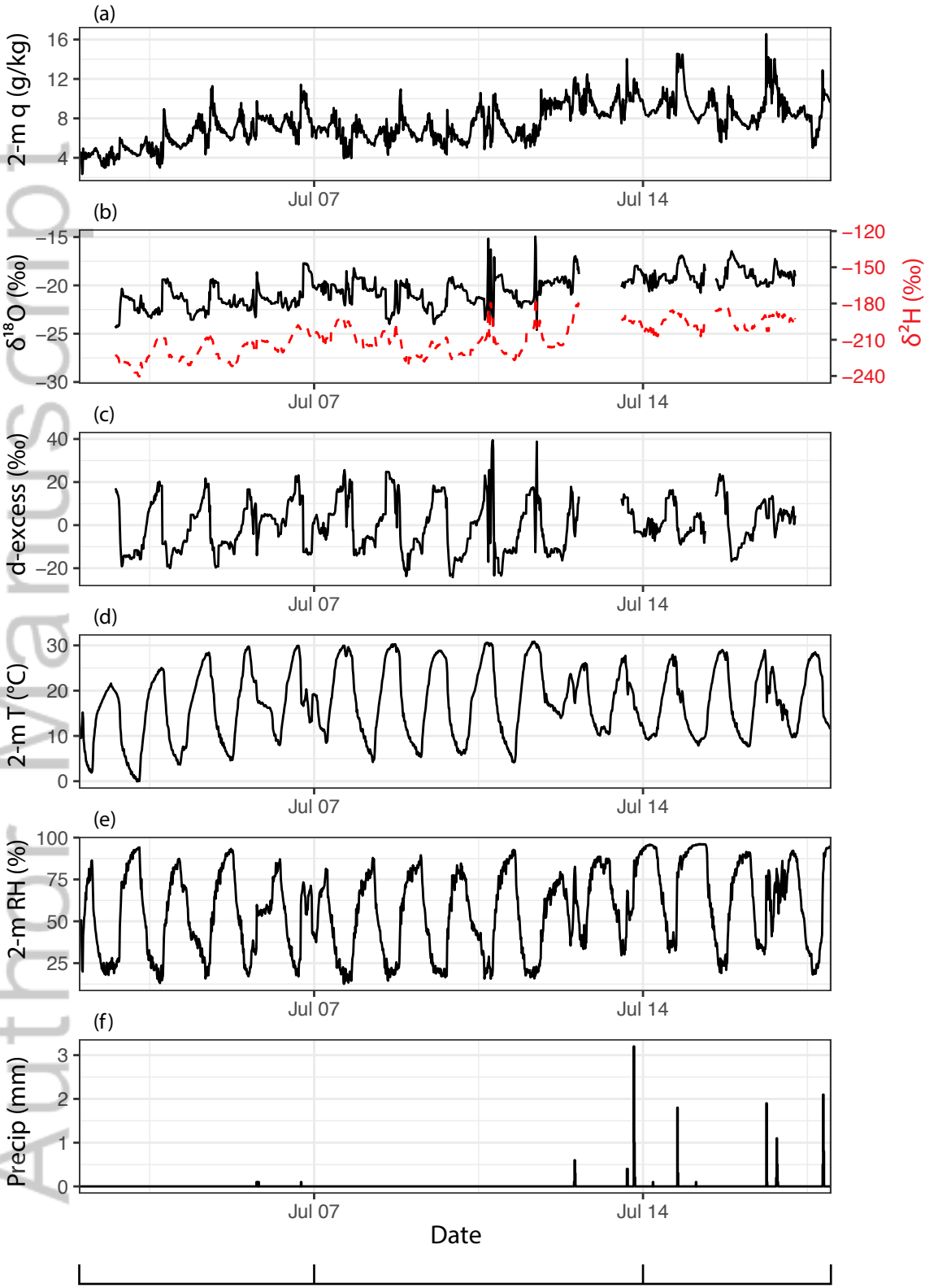

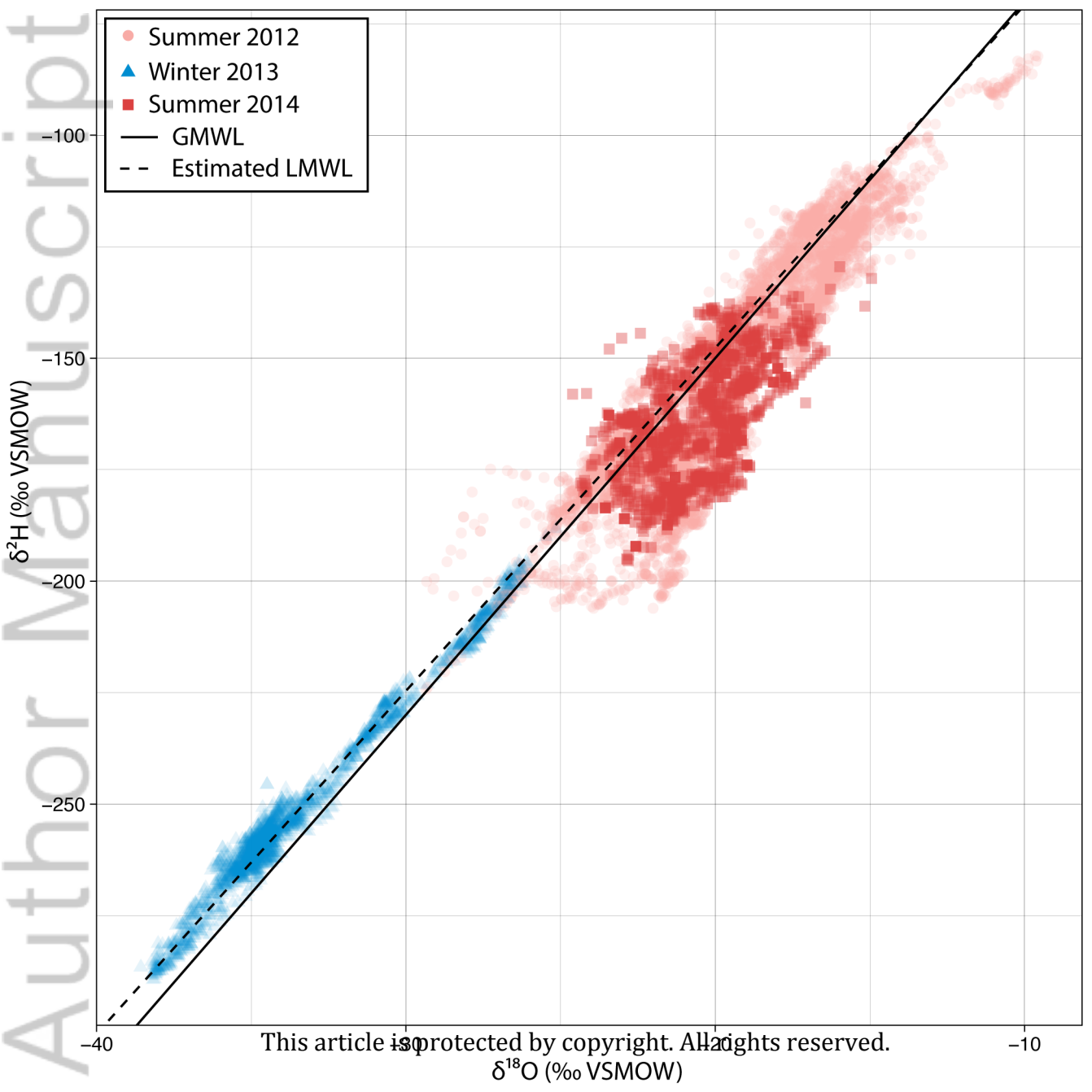

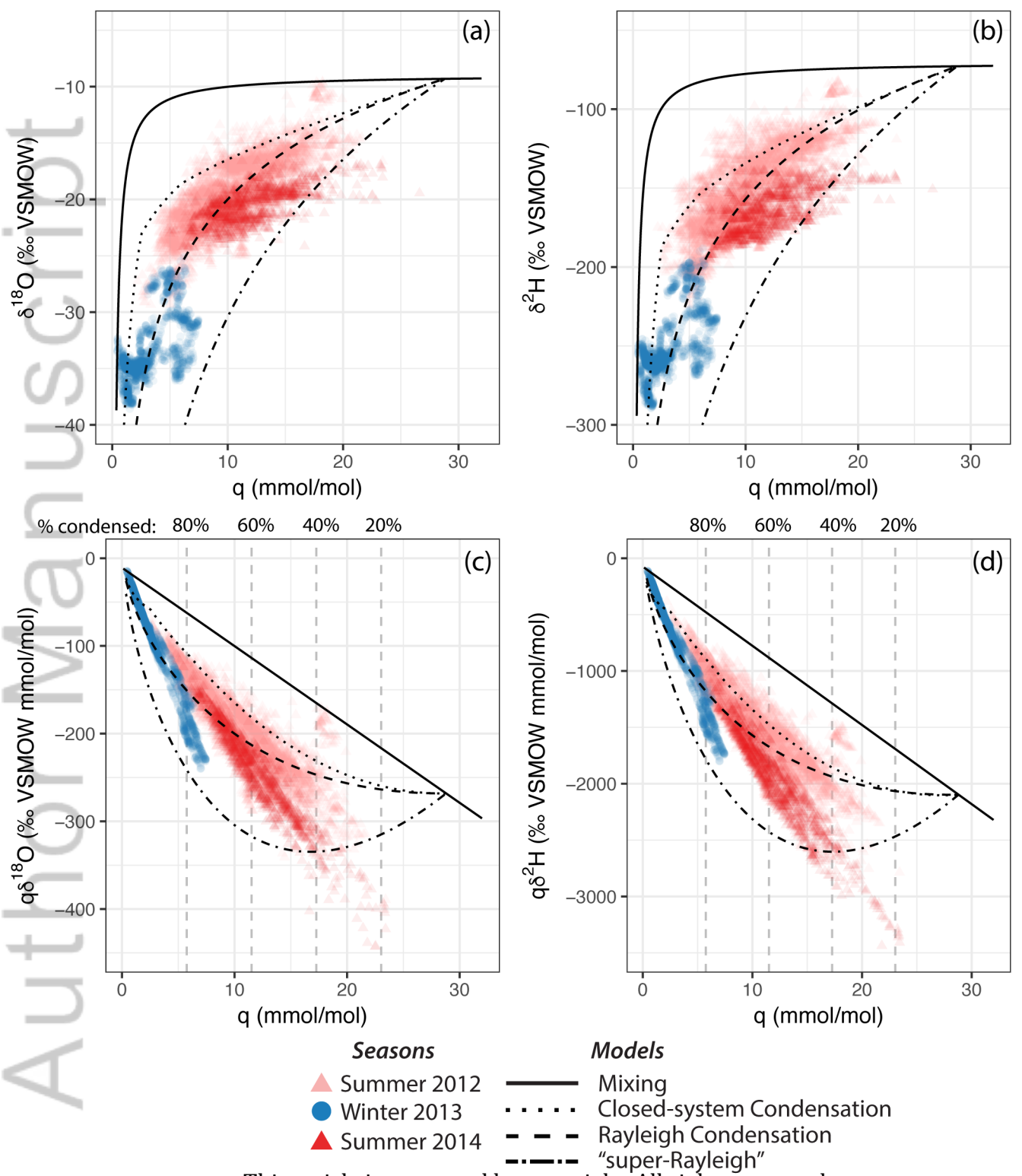

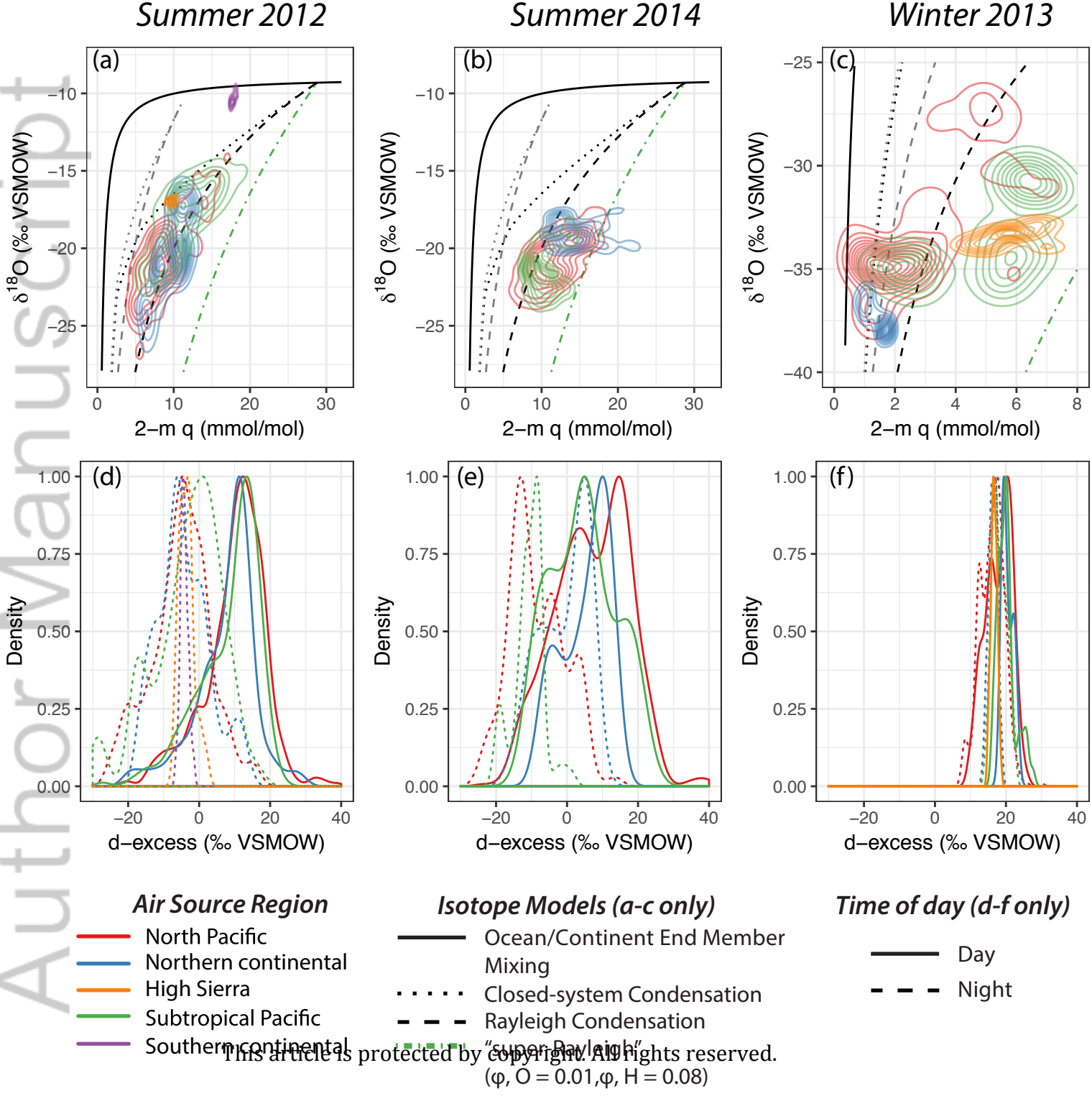

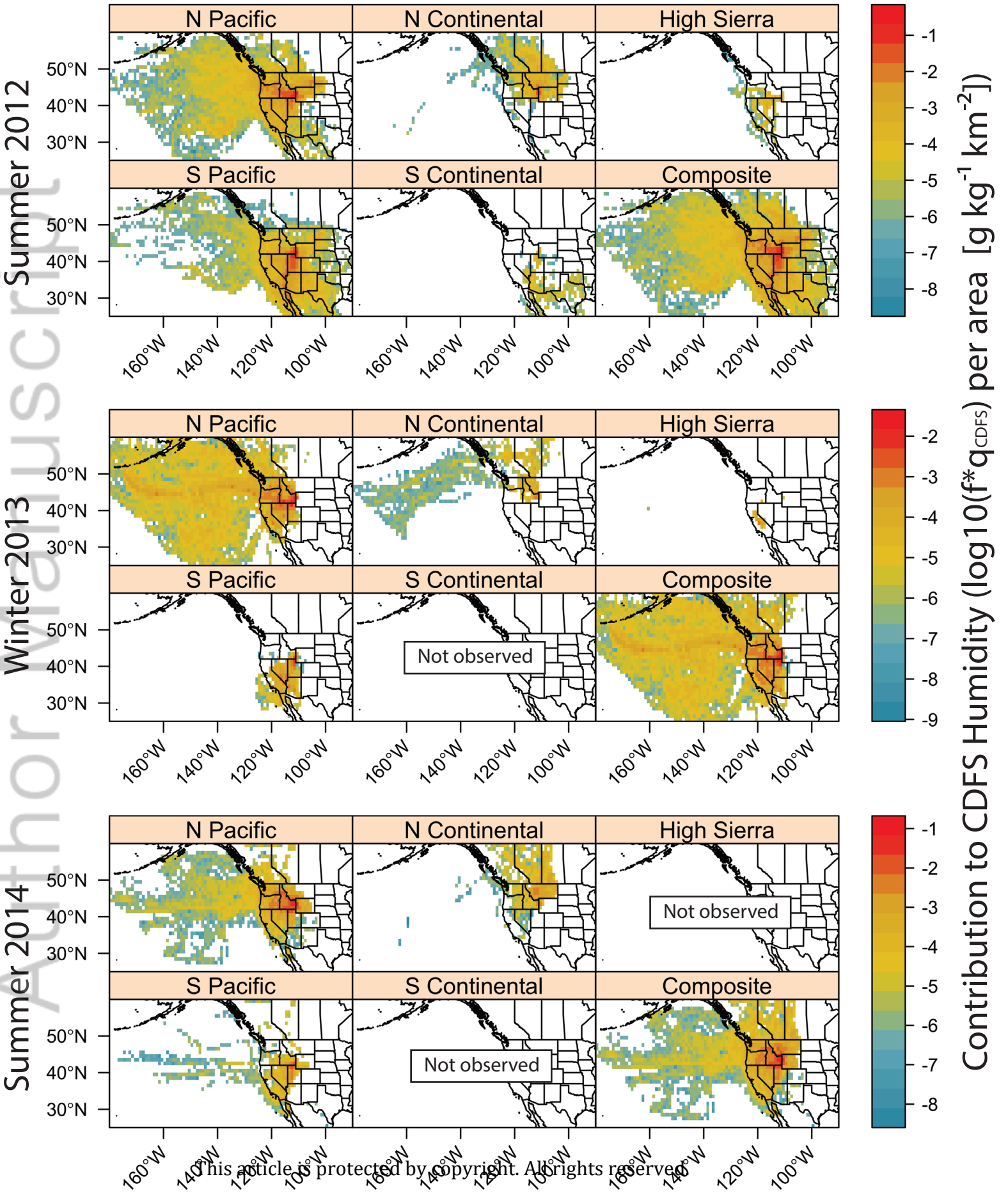

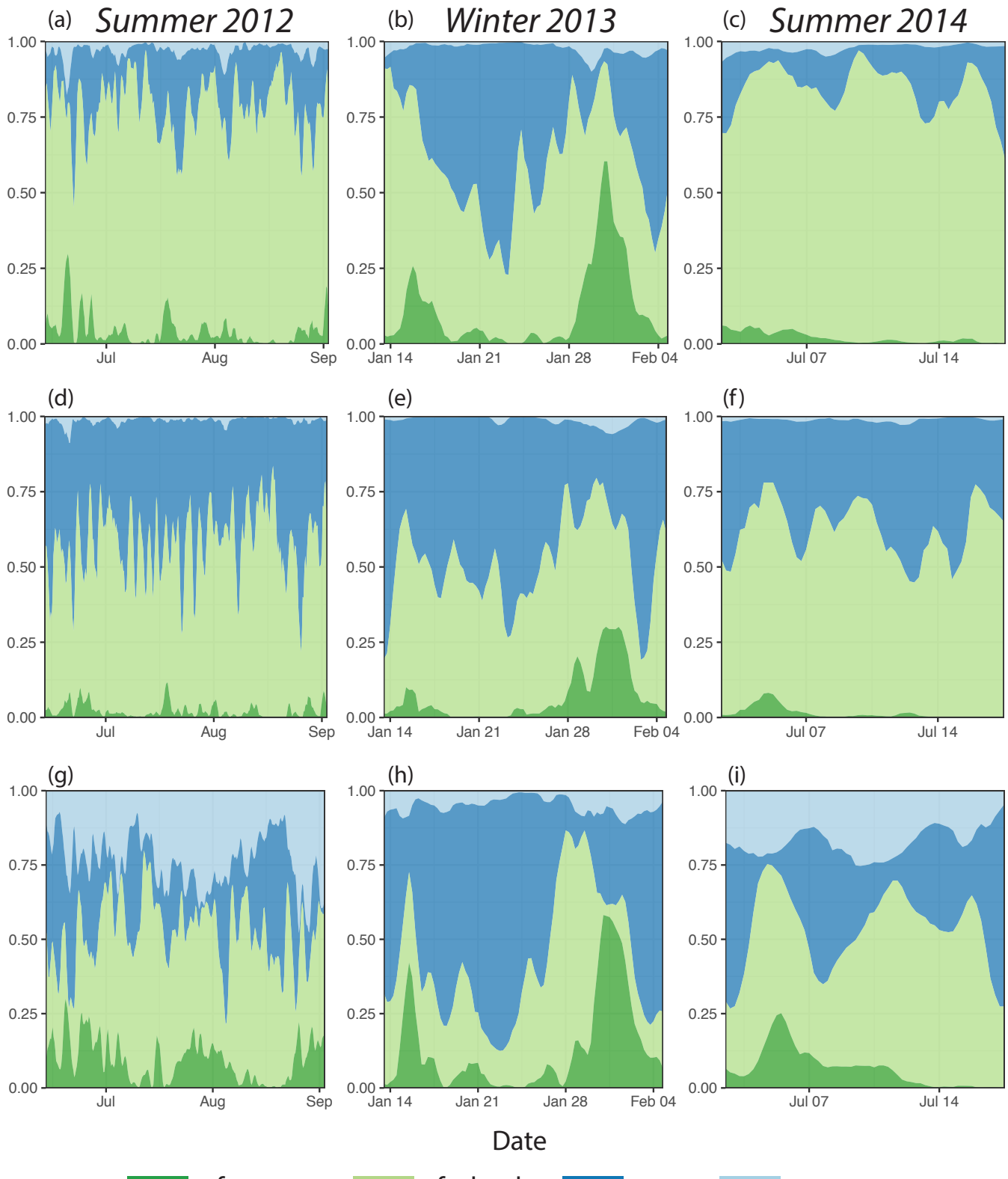

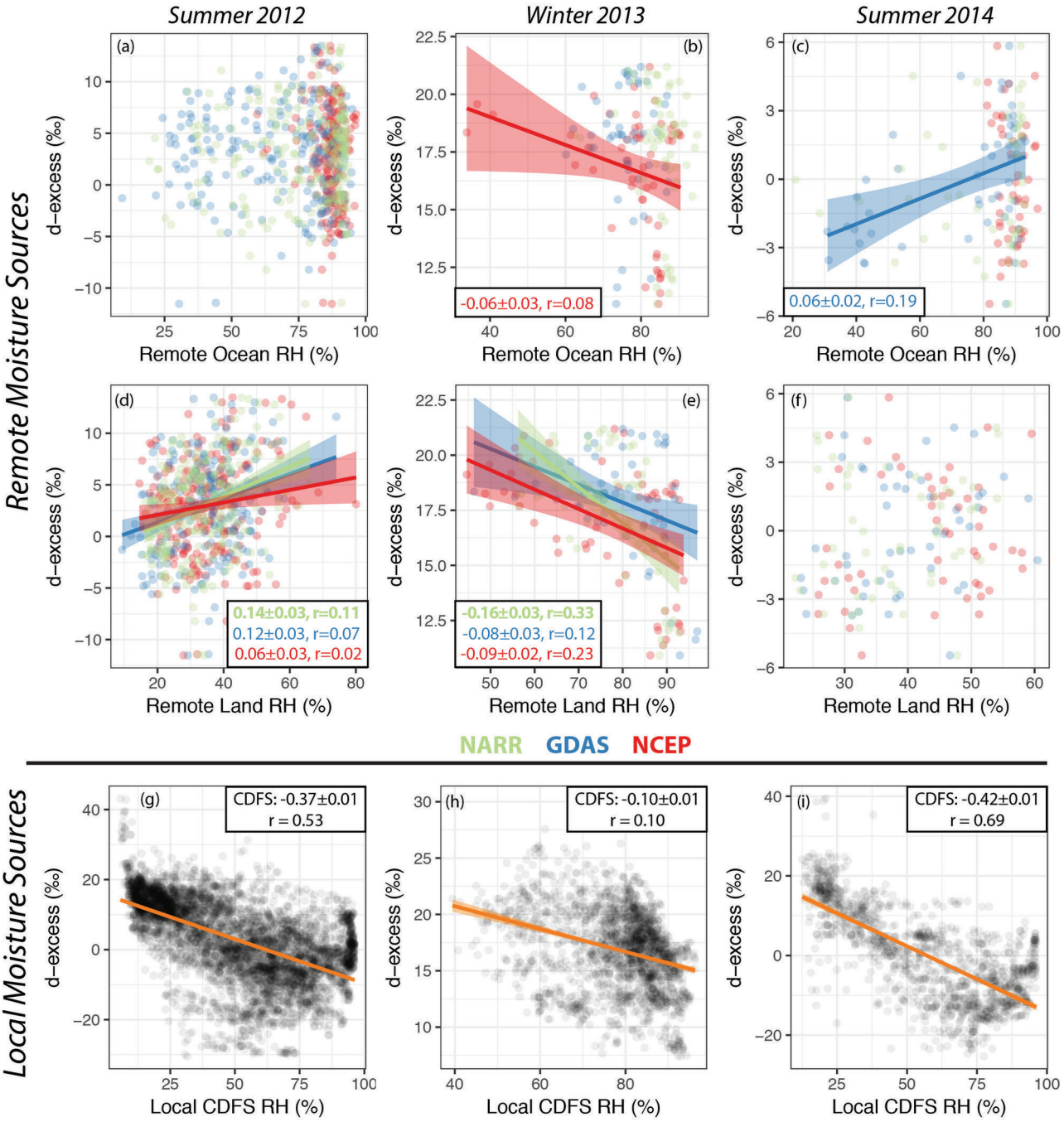

2017JD028093-f10-z-.jpg